

Single-Step Bidirectional Unpaired Image Translation Using Implicit Bridge Consistency Distillation

Suhyeon Lee^{1*}, Kwanyoung Kim^{2*}, Jong Chul Ye¹

Kim Jae Chul Graduate School of AI, KAIST¹, Samsung Research²

suhyeon.lee@kaist.ac.kr, k.0.kim@samsung.com, jong.ye@kaist.ac.kr

Abstract

Unpaired image-to-image translation has seen significant progress since the introduction of CycleGAN. However, methods based on diffusion models or Schrödinger bridges have yet to be widely adopted in real-world applications due to their iterative sampling nature. To address this challenge, we propose a novel framework, Implicit Bridge Consistency Distillation (IBCD), which enables single-step bidirectional unpaired translation without using adversarial loss. IBCD extends consistency distillation by using a diffusion implicit bridge model that connects PF-ODE trajectories between distributions. Additionally, we introduce two key improvements: 1) distribution matching for consistency distillation and 2) adaptive weighting method based on distillation difficulty. Experimental results demonstrate that IBCD achieves state-of-the-art performance on benchmark datasets in a single generation step. Project page available at: https://hyn2028.github.io/project_page/IBCD/index.html

1. Introduction

Unpaired image-to-image translation [37, 50], which transfers images between domains while preserving content without supervision, has gained continuous attention in academia and industry. This approach is particularly useful in real-world scenarios where paired data is hard to obtain, such as in medical and scientific imaging [3, 15]. However, due to the lack of foundational models and challenges with latent models in ensuring detail accuracy, modern zero-shot image editing methods [11, 12, 29] are difficult to apply. As such, unpaired image-to-image translation is essential for applications like image enhancement, artifact removal, and cross-modality translation in modern computer vision [32].

Traditionally, CycleGAN [21, 50] and its GAN-based derivatives form the foundation for unpaired image-to-image translation [6, 9, 27, 48]. These methods use bidirectional generators to translate images between domains and domain-specific discriminators. The training process com-

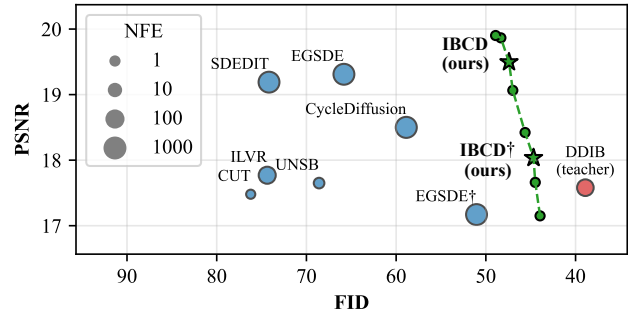


Figure 1. PSNR-FID trade-off comparison with baselines on the Cat→Dog task. The size of the marker represents the NFE.

bines adversarial loss, with feedback from the discriminators, and cycle consistency loss, enabled by the bidirectional architecture. While CycleGAN-based methods have significantly advanced unpaired image-to-image translation, they still rely on adversarial loss, which can cause issues such as training instability, convergence difficulties, and mode collapse [31]. Moreover, the performance of traditional CycleGAN-based methods falls far behind that of modern generative models.

The recent emergence of diffusion models (DMs) has significantly advanced unpaired image-to-image translation, thanks to their exceptional generative capabilities through iterative denoising. SDEdit [25], perform image translation by solving the reverse SDE with a diffusion model trained on the target domain. This is achieved by introducing noise to the source image or mapping it to a noisy space using an inversion-like method [43]. Additionally, a regularizer is introduced to balance the realism-faithfulness tradeoff [38, 46]. On the other hand, Schrödinger Bridge [33] offers a promising approach for translating between two arbitrary distributions using entropy-regularized optimal transport. Various methods have been developed for translating between data distributions, such as those proposed in [4, 23, 40], though many of these methods are limited to paired settings. In contrast, DDIB [37] addresses image-to-image translation by concatenating the ODE trajectories of two distinct DMs,

Table 1. A systematic comparison of IBCD with other diffusion-based image-to-image translation models highlights several key advantages of our approach.

Model	Single-step	Unpaired	Bi-direction	Discriminator
SDEdit [25]	✗	✓	✗	✗
EGSDE [46]	✗	✓	✗	✗
CycleDiffusion [43]	✗	✓	✓	✗
DDIB [37]	✗	✓	✓	✗
DDBM [49]	✗	✗	✓	✗
UNSB [18]	✗	✓	✗	✓
IBCD (Ours)	✓	✓	✓	✗

making it suitable for unpaired settings, yet it still relies on numerous iterative steps. More recently, UNSB [18] has been introduced to directly tackle unpaired image-to-image translation by regularizing Sinkhorn paths. Despite the aforementioned advancements in diffusion-based approaches, there still exist challenges encountered by particularly the inference cost associated with their fundamental iterative nature, which limits their practical usability.

To address the limitations, we aim at the development of a bidirectional *single-step* generator that enables translation between two arbitrary distributions in unpaired settings without relying on adversarial losses (see a comparison in Tab. 1). Specifically, we propose Implicit Bridge Consistency Distillation (IBCD), an extension of the concept of consistency distillation (CD) [36] that incorporates a diffusion implicit bridge model for translating between arbitrary data distributions. Unlike CD, which learns paths from Gaussian noise to data, IBCD connects trajectories from one arbitrary distribution to another one using a Probability Flow Ordinary Differential Equation (PF-ODE), allowing for flexible and efficient distribution translation.

However, simply extending CD can result in reduced distillation efficacy due to error accumulation, as well as challenges related to model capacity and training scheme, which arise from integrating two trajectories and introducing bidirectionality. To address this, we propose a regularization method called Distribution Matching for Consistency Distillation (DMCD). Furthermore, we introduce a novel weighting scheme based on distillation difficulty, which applies a stronger DMCD penalty specifically to samples where the consistency loss alone proves insufficient. By integrating additional cycle translation loss with these advanced components, our approach significantly enhances the realism-faithfulness trade-off, achieving state-of-the-art performance in a single step, as shown in Fig. 1. The main contributions of our work are as follows:

- We propose Implicit Bridge Consistency Distillation (IBCD), a novel unpaired image translation framework enabling bidirectional translation with a single NFE, achieving state-of-the-art results.
- We introduce further improvements, including Distribution Matching for Consistency Distillation (DMCD), an adaptive weighting scheme based on distillation diffi-

culty, and cycle translation loss to effectively mitigate inherent distillation errors.

2. Preliminaries

2.1. Image Translation with Diffusion Models

Diffusion Models (DM). In DMs [14, 35], the predefined forward process with the time variable $t \in [0, T]$ progressively corrupts data into pure Gaussian noise over a series of steps T . Specifically, given a data distribution $\mathbf{x}_0 \sim p(\mathbf{x}_0) := p_{\text{real}}(\mathbf{x})$, the distribution $\mathbf{x}_T \sim p(\mathbf{x}_T)$ approaches an isotropic normal distribution as noise is added according to the process $p(\mathbf{x}_t | \mathbf{x}_0) = \mathcal{N}(\mathbf{x}_0, t^2 \mathbf{I})$. The reverse of this process can be described by an SDE or a PF-ODE [35] as follows:

$$\frac{d\mathbf{x}_t}{dt} = -t \nabla_{\mathbf{x}_t} \log p(\mathbf{x}_t) = \frac{\mathbf{x}_t - \mathbb{E}[\mathbf{x}_0 | \mathbf{x}_t]}{t}, \quad (1)$$

where the second equality follows from Tweedie’s formula, $\mathbb{E}[\mathbf{x}_0 | \mathbf{x}_t] = \mathbf{x}_t + t^2 \nabla_{\mathbf{x}_t} \log p(\mathbf{x}_t)$ [8, 20]. In practice, the neural network is trained to approximate the ground truth score function $\mathbf{s}_\phi(\mathbf{x}_t, t) \approx \nabla_{\mathbf{x}_t} \log p(\mathbf{x}_t)$ or the denoiser $D_\phi(\mathbf{x}_t, t) \approx \mathbb{E}[\mathbf{x}_0 | \mathbf{x}_t]$ by denoising score matching [39]. By substituting the trained neural networks into Eq. (1), we can obtain the denoised sample by numerically integrating from T to 0:

$$\mathbf{x}_0 = \mathbf{x}_T + \int_T^0 -t \cdot \mathbf{s}_\phi(\mathbf{x}, t) dt \quad (2)$$

To solve Eq. (2), an ODE solver, denoted as $\text{Solve}(\mathbf{x}_T; \phi, T, 0)$ (with an initial state \mathbf{x}_T at time T and ending at time 0, DM parameterized by ϕ) can be applied. Examples include the Euler solver [14, 35], DPM-solver [24], or the second-order Heun solver [17]. The sampling process typically requires dozens to hundreds of neural function evaluations (NFE) to effectively minimize discretization error during ODE solving.

Dual Diffusion Implicit Bridge (DDIB). DDIB [37] is a simple yet effective method for image-to-image translation that leverages the connection between DMs and Schrödinger bridge problem (SBPs), where DMs act as implicit optimal transport models. DDIB requires training two individual DMs for the two domains A and B, denoted as \mathbf{s}_{ϕ^a} and \mathbf{s}_{ϕ^b} . The sampling process involves sequential ODE solving as follows:

$$\mathbf{x}^l = \text{Solve}(\mathbf{x}^a; \phi^a, 0, T), \mathbf{x}^b = \text{Solve}(\mathbf{x}^l; \phi^b, T, 0). \quad (3)$$

Here, \mathbf{x}^l represents the latent code in the pure Gaussian noise domain, \mathbf{x}^a is the image in the source domain, and \mathbf{x}^b is the estimated image in the target domain. Thanks to the intermediate Gaussian distribution, DDIB automatically satisfies the cycle consistency property without requiring any explicit regularization term [6, 51].

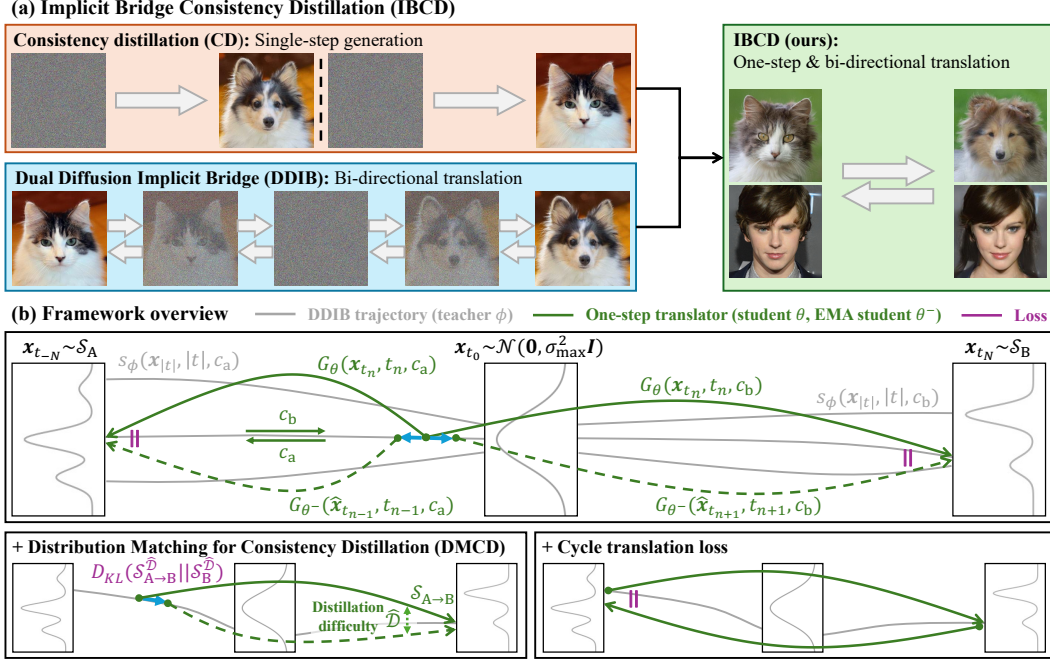


Figure 2. (a) IBCD performs single-step bi-directional translation using a distillation framework that extends consistency distillation with a diffusion implicit bridge. (b) The IBCD framework bridges two distributions by connecting the PF-ODE paths of two pre-trained diffusion models through bidirectionally extended consistency distillation. To mitigate distillation errors, we introduce distribution matching for consistency distillation and a cycle translation loss.

2.2. Existing Single-Step Acceleration Approaches

Consistency Distillation (CD). The aim of the consistency distillation (CD) [36] is to learn the direct mapping from noise to clean data. Specifically, the model is designed to predict $f_\theta(\mathbf{x}_t, t) = \mathbf{x}_0$, and is constrained to be *self-consistent*, meaning that outputs should be the same for any time point input within the same PF-ODE trajectory, *i.e.*, $f(\mathbf{x}_t, t) = f(\mathbf{x}_{t'}, t')$ for all $t, t' \in [\epsilon, T]$, with the boundary condition $f_\theta(\mathbf{x}_\epsilon, \epsilon) = \mathbf{x}_\epsilon$. Here, ϵ is a small positive number, to avoid numerical instability at an $t = 0$. By discretizing the time interval $[\epsilon, T]$ into $N - 1$ sub-interval with boundaries $t_1 = \epsilon < t_2 < \dots < t_N = T$, the resulting objective function for CD is given by:

$$\mathcal{L}_{CD}(\theta; \phi) = \mathbb{E}[\lambda(t_n)d(f_\theta(\mathbf{x}_{t_{n+1}}, t_{n+1}), f_{\theta^-}(\hat{\mathbf{x}}_{t_n}, t_n))],$$

where $n \sim \mathcal{U}[1, N - 1]$ and $\lambda(t_n)$ is weight hyperparameter, $d(\cdot, \cdot)$ measures the distance between two samples. θ^- is the exponential moving average (EMA) of the student parameter θ , and ϕ represents the pre-trained teacher model, and $\mathcal{U}[\cdot]$ refers to the uniform distribution. The target $\hat{\mathbf{x}}_{t_n}$ is obtained by solving one-step ODE solver, *i.e.*, $\hat{\mathbf{x}}_{t_n} = \text{Solve}(\mathbf{x}_{t_{n+1}}; \phi, t_{n+1}, t_n)$, from $\mathbf{x}_{t_{n+1}} \sim \mathcal{N}(\mathbf{x}_0, t_{n+1}^2 \mathbf{I})$.

Distribution Matching Distillation (DMD). DMD [42, 44] minimizes the Kullback-Leibler (KL) divergence between the real data distribution, p^{real} , and the student sample distribution, p_θ^{fake} in order to distill the diffusion model

s_ϕ^{real} into a single-step generator $f_\theta(\mathbf{x}_T) = \mathbf{x}_0$. Additionally, DMD introduces an auxiliary “fake” DM, s_ψ^{fake} , to approximate the score function of the student-generated sample distribution, which is otherwise inaccessible. This estimator is trained with denoising score matching, adapting in real-time as the student model progresses through training. The gradient of the DMD loss is then approximated as the difference between the two score functions:

$$\begin{aligned} \nabla_\theta D_{KL}(p_\theta^{\text{fake}} || p^{\text{real}}) &\approx \nabla_\theta \mathcal{L}_{DMD} \\ &= \mathbb{E}_{\mathbf{x}_t, t, \mathbf{x}_T} [w_t (s_\psi^{\text{fake}}(\mathbf{x}_t, t) - s_\phi^{\text{real}}(\mathbf{x}_t, t)) \nabla_\theta f_\theta(\mathbf{x}_T)] \end{aligned} \quad (4)$$

where $\mathbf{x}_t \sim \mathcal{N}(f_\theta(\mathbf{x}_T), t^2 \mathbf{I})$, $t \sim \mathcal{U}(T_{\min}, T_{\max})$, $\mathbf{x}_T \sim \mathcal{N}(\mathbf{0}, T^2 \mathbf{I})$ and w_t is a scalar weighting factor. DMD serves as an effective distillation loss that optimizes the student model from the view of the distribution, without the need to rely on the instability related with adversarial loss [10].

3. Main Contribution

We aim to develop a single-step distillation method for bi-directional mapping between arbitrary distributions in an unpaired setting, using pre-trained diffusion models. Specifically, given two domains \mathcal{X}_A and \mathcal{X}_B with unpaired datasets \mathcal{S}_A and \mathcal{S}_B , our translator f_θ performs two translations: $f_\theta(\mathbf{x}^a, c_b)$ for $A \rightarrow B$ and $f_\theta(\mathbf{x}^b, c_a)$ for $B \rightarrow A$, where c_a and c_b are class embeddings for the target translation domain.

The main concept of our method is illustrated in Fig. 2 by contrasting it to the DDIB [37]. In the following, we describe a novel distillation approach with distribution matching, adaptive weighting, and a cycle loss for bidirectional reconstruction.

3.1. Implicit Bridge Consistent Distillation

Definition. Our model architecture and diffusion process are based on the PF-ODE using EDM [17]. To handle both domains with one generator, a pre-trained class conditional DMs, $s_\phi(\mathbf{x}_t, t, c)$, is jointly trained for each domain with class conditions c_a and c_b . Specifically, the teacher model s_ϕ is trained using denoising score matching (DSM) for continuous-time $t = \sigma \sim \text{Lognormal} \in (0, \infty)$ without any modification from EDM. The timestep discretization for the sampling process is defined as $[t_0, t_1, \dots, t_i, \dots, t_N] = [\sigma_{\max}, \sigma_{\max-1}, \dots, \sigma_{\min}, 0]$. Since DDIB concatenates two independent ODEs into a single ODE, duplicated timesteps must be redefined for consistency distillation (CD). We introduce a unique discretized timestep index i and redefine the timestep t for the concatenated trajectory ($\mathcal{X}_A \leftrightarrow \mathcal{X}_B$) as follows:

$$i = \underbrace{[-N, -N+1, \dots, -1]}_{\mathcal{X}_A}, \underbrace{0}_{\mathcal{X}_A \cap \mathcal{X}_B}, \underbrace{1, \dots, N-1, N}_{\mathcal{X}_B}$$

$$t_i = [-0, -\sigma_{\min}, \dots, -\sigma_{\max-1}, +\sigma_{\max}, +\sigma_{\max-1}, \dots, +\sigma_{\min}, +0] \quad (5)$$

Boundary Condition. Given that the student model’s output is enforced to be *self-consistent* with respect to timesteps in Eq. (5), we define the student as $f_\theta(\mathbf{x}_t, t, c)$, where t is a non-zero real-valued timestep and $c \in c_a, c_b$ represents the target domain condition. For simplicity, we denote the opposite class embedding as c' , such that when $c = c_b$, $c' := c_a$. To enable bidirectional translation, we redefine the boundary condition of IBCD to depend on the target domain condition c :

$$f(\mathbf{x}_{\epsilon(c)}, \epsilon(c), c) = \mathbf{x}_{\epsilon(c)},$$

$$\text{where } \epsilon(c) = \begin{cases} t_{-N+1} & = -\sigma_{\min}, & \text{for } c = c_a \\ t_{N-1} & = +\sigma_{\min}, & \text{for } c = c_b \end{cases}. \quad (6)$$

This boundary condition, along with the IBCD loss introduced later, allows translation by injecting the desired domain condition: $f(\mathbf{x}_{\epsilon(c)}, \epsilon(c), c') = \mathbf{x}_{\epsilon(c')}$, where $f(\mathbf{x}_t, t, c_b)$ transforms \mathbf{x}_t at any t between \mathcal{X}_A and \mathcal{X}_B into a clean domain \mathcal{X}_B image $\mathbf{x}_{t_{N-1}}$ belonging to the same ODE trajectory, and vice versa. Since EDM/CD is not defined for negative t values and does not directly align with our new boundary conditions, we extend the EDM/CD formulation and apply it to the student model¹. For more details on this extension, refer to Appendix B.

¹Note that this formulation applies exclusively to the student model.

The Method. To generate data pairs $(\mathbf{x}_{t_1}, \hat{\mathbf{x}}_{t_2})$ that belong to the same PF-ODE trajectory for IBCD, we perform forward diffusion on the dataset and predict the next data point one step ahead using a suitable teacher model and ODE solver. For simplicity, we denote the teacher model ϕ conditioned on class c as ϕ^c . The data pair generation process in the direction of $\mathcal{X}_A \rightarrow \mathcal{X}_B$ (i.e. $c = c_b$) for each domain is as follows:

$$\hat{\mathbf{x}}_{t_{n_a+1}} = \text{Solve}(\mathbf{x}_{t_{n_a}}; \phi^a, |t_{n_a}|, |t_{n_a+1}|),$$

$$\hat{\mathbf{x}}_{t_{n_b+1}} = \text{Solve}(\mathbf{x}_{t_{n_b}}; \phi^b, |t_{n_b}|, |t_{n_b+1}|), \quad (7)$$

where $n_a \sim \mathcal{U}[-N+1, -1]$, $n_b \sim \mathcal{U}[0, N-2]$, $\mathbf{x}_{t_{n_a}} \sim \mathcal{N}(\mathbf{x}^a, t_{n_a}^2 \mathbf{I})$, $\mathbf{x}_{t_{n_b}} \sim \mathcal{N}(\mathbf{x}^b, t_{n_b}^2 \mathbf{I})$. Similarly, in the direction $\mathcal{X}_B \rightarrow \mathcal{X}_A$ (i.e. $c = c_a$), the data pair for each domain can be generated as:

$$\hat{\mathbf{x}}_{t_{n_a-1}} = \text{Solve}(\mathbf{x}_{t_{n_a}}; \phi^a, |t_{n_a}|, |t_{n_a-1}|),$$

$$\hat{\mathbf{x}}_{t_{n_b-1}} = \text{Solve}(\mathbf{x}_{t_{n_b}}; \phi^b, |t_{n_b}|, |t_{n_b-1}|), \quad (8)$$

where $n_a \sim \mathcal{U}[-N+2, 0]$, $n_b \sim \mathcal{U}[1, N-1]$. Given these distillation targets, our objective function of IBCD is defined as follows:

$$\mathcal{L}_{\text{IBCD}}(\theta; \phi) = \mathbb{E}_{\mathbf{t}_1, \mathbf{x}_{\mathbf{t}_1}, c} [\lambda(\mathbf{t}_2) d(f_\theta(\mathbf{x}_{\mathbf{t}_1}, \mathbf{t}_1, c), f_{\theta^-}(\hat{\mathbf{x}}_{\mathbf{t}_2}, \mathbf{t}_2, c))], \quad (9)$$

where $\mathbf{x}_{\mathbf{t}_1} = [\mathbf{x}_{t_{n_a}}; \mathbf{x}_{t_{n_b}}]$, $\hat{\mathbf{x}}_{\mathbf{t}_2} = [\hat{\mathbf{x}}_{t_{n_a \pm 1}}; \hat{\mathbf{x}}_{t_{n_b \pm 1}}]$, $c \in \mathcal{U}[\{c_a, c_b\}]$, $\mathbf{t}_1 = [t_{n_a}; t_{n_b}]$, $\mathbf{t}_2 = [t_{n_a \pm 1}; t_{n_b \pm 1}]$, $\theta^- = \text{sg}(\mu\theta^- + (1-\mu)\theta)$. $n_{(\cdot) \pm 1}$ denotes time index for each distillation direction in Eqs. (7), (8) and sg indicates the stop-gradient operator. For a detailed explanation, see Algo. 1.

Using a single domain-independent teacher model instead of two reduces memory consumption and provides an effective initializer for the student model, acting as a unified model for both domains. By sharing the class condition in the teacher and the target domain condition in the student as a unified embedding, we can leverage the student’s initialization weights, as $f(\mathbf{x}_t, t, c)$ is designed to output a clean image for domain c . This approach differs from methods in the literature [19, 22], which extend CD in both directions or specify a target timestep, but don’t fully integrate domain conditions into a cohesive framework.

3.2. Objective Function

There are still some challenges in enabling single-step bidirectional transport of the student model in unpaired settings.

First, the consistency loss relies on a local strategy (categorized by Kim et al. [19]), aligning consistency only between adjacent timesteps using the student’s output recursively. This can lead to accumulating local errors, causing a growing discrepancy between the student’s prediction $f_\theta(\mathbf{x}_t, t, c)$ and the true boundary value $\mathbf{x}_{\epsilon(c)}$ as the distance from the boundary condition timestep doubles. This

issue is amplified in IBCD due to its doubling trajectory compared to standard CD. Second, the student must manage both bidirectional tasks and learn two distinct ODE trajectories. Since the teacher’s ODEs share timesteps but differ only in conditions, this added complexity can strain model capacity, complicating training. Similar performance degradation from bidirectional tasks has been observed in CD by Li and He [22]. Finally, unlike EGSDE [46], which adjusts the trade-off between realism and fidelity by weighting expert contributions, vanilla IBCD lacks a mechanism to control this balance, limiting its adaptability.

Distribution Matching for Consistency Distillation (DMCD). To address these issues, we propose Distribution Matching for Consistency Distillation (DMCD), which extends the DMD loss to fit within the CD framework. DMCD builds on the DMD loss by optimizing the KL divergence between the student’s output samples and the target domain data distributions across all timesteps in bidirectional tasks. Furthermore, it incorporates the distillation difficulty adaptive weighting factor $\hat{\mathcal{D}}(\cdot, \cdot)$. This adaptive weighting scheme helps to focus the optimization on challenging samples, thereby enhancing the overall performance and stability of the student model during training. The resulting DMCD is given by:

$$\begin{aligned} \nabla_{\theta} \mathcal{L}_{\text{DMCD}} = & \mathbb{E}_{\mathbf{t}_1, \mathbf{x}_{\mathbf{t}_1}, c, i, \mathbf{x}_{t_i}} [w_{t_i} \hat{\mathcal{D}}(\text{sg}(\mathbf{x}_{\mathbf{t}_1}), c) \cdot \\ & (s_{\psi}(\mathbf{x}_{t_i}, t_i, c) - s_{\phi}(\mathbf{x}_{t_i}, t_i, c)) \nabla_{\theta} f_{\theta}(\mathbf{x}_{\mathbf{t}_1}, \mathbf{t}_1, c)] \quad (10) \\ \text{where } & i \sim \mathcal{U}[0, N - 1], \mathbf{x}_{t_i} \sim \mathcal{N}(f_{\theta}(\mathbf{x}_{\mathbf{t}_1}, \mathbf{t}_1, c), t_i^2 \mathbf{I}) \end{aligned}$$

where $\mathbf{t}_1, \mathbf{x}_{\mathbf{t}_1}, c$ are defined per from Eq. (9), and w represents a time-dependent weighting factor introduced in DMD. The term $s_{\psi}(\mathbf{x}_t, t, c)$ denotes a class-conditional fake diffusion model, which is continuously trained via DSM on outputs of student f_{θ} , adapting as the training progresses. Unlike DMD, DMCD functions as a regularizer rather than the primary objective. This distinction is crucial in unpaired settings, where relying solely on the DMCD loss does not ensure a proper connection between two domains. IBCD bridges a trajectory between two distributions using consistency loss, while DMCD addresses the distribution matching issue, working as a regularizer to increase the realism of the results. This integration allows for improved performance and stability without the drawbacks associated with adversarial training like [18, 30, 51].

Distillation Difficulty Adaptive Weighting. DMCD effectively brings the translated distribution closer to the target data distribution, enhancing the realism of the generated samples. However, this can also cause a divergence from the teacher model’s estimations, thereby reducing faithfulness to the source distribution. Ideally, DMCD should be applied more intensively to challenging PF-ODE trajectories that the student model struggles to translate accurately, particularly those involving source domain data points near

the decision boundary of the source domain.

To address this, we propose a *distillation difficulty adaptive weighting* strategy. To quantify the difficulty, we introduce the concept of *distillation difficulty*, $\mathcal{D}([\mathbf{x}_{t_{-N+1}}, \dots, \mathbf{x}_{t_{N-1}}], c) := d(f_{\theta}(\mathbf{x}_{\epsilon(c')}, \epsilon(c'), c), \mathbf{x}_{\epsilon(c)})$, which measures the challenge of distilling a given ODE trajectory generated by the teacher between domains. This approach ensures that DMCD is applied more aggressively to the most difficult trajectories, improving the overall translation performance by focusing on areas where the student model needs it the most. Such a strategy could strike a balance between source faithfulness and realism by applying the DMCD loss forcefully only to trajectories where the IBCD loss alone is insufficient. However, estimating $\mathbf{x}_{\epsilon(c)}$ and $\mathbf{x}_{\epsilon(c')}$ from a given \mathbf{x}_t using the ODE solver requires at least N NFEs with the teacher model for each DMCD loss calculation, which is computationally impractical. To address this, we propose a one-step approximation of the weighting factor $\mathcal{D}(\cdot, \cdot)$, defined as follows:

$$\hat{\mathcal{D}}(\mathbf{x}_{\mathbf{t}_1}, c) = g(d(f_{\theta}(\mathbf{x}_{\mathbf{t}_1}, \mathbf{t}_1, c), f_{\theta}(\hat{\mathbf{x}}_{\mathbf{t}_2}, \mathbf{t}_2, c))) \quad (11)$$

where $\mathbf{t}_1, \mathbf{t}_2, \mathbf{x}_{\mathbf{t}_1}, \hat{\mathbf{x}}_{\mathbf{t}_2}$ are defined in Eqs. (9), (10) and g is any monotone increasing function. The validity of the alternative weighting factor will be confirmed later through experiments.

Cycle Consistency Loss. Similar to DDIB, our framework is designed to perform cycle translation and must therefore satisfy cycle consistency. The objective function of enforcing this requirement can be expressed as $\mathcal{L}_{\text{cycle}}$:

$$\mathbb{E}_{c, \mathbf{x}_{\epsilon(c)}} [d(f_{\theta}(f_{\theta}(\mathbf{x}_{\epsilon(c)}, \epsilon(c), c'), \epsilon(c'), c), \mathbf{x}_{\epsilon(c)})]. \quad (12)$$

Final Loss Functions. The final loss, weighted by $\lambda_{\text{DMCD}}, \lambda_{\text{cycle}}$, for training f_{θ} is given by:

$$\theta^* = \arg \min_{\theta} \mathcal{L}_{\text{IBCD}} + \lambda_{\text{DMCD}} \mathcal{L}_{\text{DMCD}} + \lambda_{\text{cycle}} \mathcal{L}_{\text{cycle}}. \quad (13)$$

Empirically, we found that the following adaptive training strategy further improves the performing: the training process begins with only the IBCD loss; as the student model approaches convergence, the DMCD and cycle consistency losses are additionally introduced to further refine the model’s performance. Detailed training procedures and the complete algorithm can be found in Algo. 2.

4. Experiments

4.1. Toy Data Experiment

To evaluate the effectiveness of our framework in a controlled setting, we conducted bidirectional translation experiments on a two-dimensional synthetic toy dataset, where the domains A and B were represented by the S-curve and Swiss roll distributions, respectively.

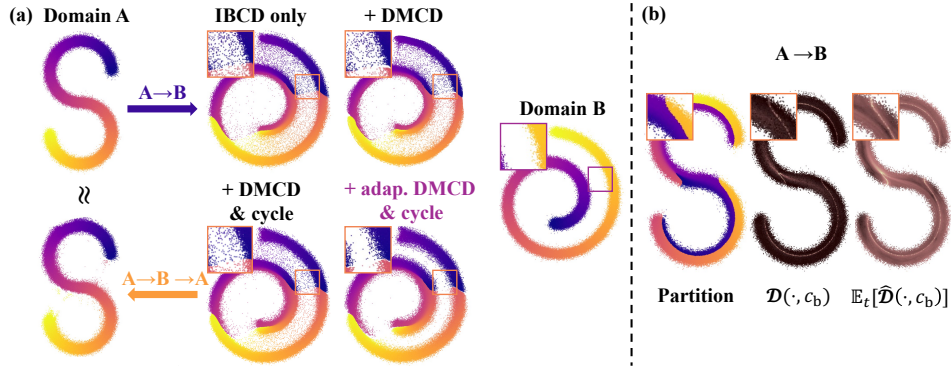


Figure 3. (a) Bidirectional translation results on a toy dataset, showing the contributions of each component. (b) Visualization of distillation difficulty $\mathcal{D}(\cdot, c_b)$ and its one-step approximation $\mathbb{E}_t[\hat{\mathcal{D}}(\cdot, c_b)]$ for $A \rightarrow B$ translation, with g selected as a logarithm.

Method	NFE ↓	FID ↓	PSNR ↑	SSIM ↑	Density ↑	Coverage ↑
Cat→Dog						
CycleGAN [51]	1	85.9	-	-	-	-
Self-Distance [2]	1	144.4	-	-	-	-
GeGAN [9]	1	96.6	-	-	-	-
LeSeSIM [47]	1	72.8	-	-	-	-
StarGAN v2 [7]	1	54.88 ± 1.01	10.63 ± 0.10	0.270 ± 0.003	-	-
CUT [28]	1	76.21	17.48	0.601	0.971	0.696
UNSB* [18]	5	68.59	17.65	0.587	1.045	0.706
ILVR [5]	1000	74.37 ± 1.55	17.77 ± 0.02	0.363 ± 0.001	1.019 ± 0.030	0.566 ± 0.012
SDEdit [25]	1000	74.17 ± 1.01	19.19 ± 0.01	0.423 ± 0.001	0.997 ± 0.021	0.526 ± 0.014
EGSDE [46]	1000	65.82 ± 0.77	19.31 ± 0.02	0.415 ± 0.001	1.258 ± 0.027	0.634 ± 0.023
EGSDE† [46]	1200	51.04 ± 0.37	17.17 ± 0.02	0.361 ± 0.001	1.509 ± 0.038	0.823 ± 0.021
CycleDiffusion [43]	1000(+100)	58.63 ± 1.08	18.36 ± 0.04	0.537 ± 0.001	0.905 ± 0.023	0.767 ± 0.028
SDDM [38]	100	62.29 ± 0.63	-	0.422 ± 0.001	-	-
SDDM† [38]	120	49.43 ± 0.23	-	0.361 ± 0.001	-	-
DDIB* (Teacher) [37]	160	38.91	17.58	0.588	1.528	0.934
IBCD (Ours)	1	47.44 ± 0.03	19.50 ± 3e-4	0.701 ± 1e-5	1.412 ± 0.007	0.940 ± 0.003
IBCD† (Ours)	1	44.77 ± 0.07	18.04 ± 2e-4	0.663 ± 8e-6	1.542 ± 0.005	0.935 ± 0.003
Wild→Dog						
CUT [28]	1	92.94	17.20	0.592	-	-
UNSB* [18]	5	70.03	16.86	0.573	1.035	0.704
ILVR [5]	1000	75.33 ± 1.22	16.85 ± 0.02	0.287 ± 0.001	1.275 ± 0.046	0.531 ± 0.013
SDEdit [25]	1000	68.51 ± 0.65	17.98 ± 0.01	0.343 ± 0.001	1.292 ± 0.045	0.636 ± 0.018
EGSDE [46]	1000	59.75 ± 0.62	18.14 ± 0.02	0.343 ± 0.001	1.482 ± 0.018	0.683 ± 0.013
EGSDE† [46]	1200	50.43 ± 0.52	16.40 ± 0.01	0.300 ± 0.001	1.733 ± 0.022	0.782 ± 0.014
CycleDiffusion [43]	1000(+100)	58.92 ± 0.72	17.68 ± 0.03	0.458 ± 0.001	1.014 ± 0.034	0.801 ± 0.027
SDDM [38]	100	57.38 ± 0.53	-	0.328 ± 0.001	-	-
DDIB* (Teacher) [37]	160	38.59	17.03	0.552	1.594	0.924
IBCD (Ours)	1	48.60 ± 0.11	18.25 ± 2e-4	0.653 ± 2e-5	1.539 ± 0.006	0.921 ± 0.005
IBCD† (Ours)	1	46.06 ± 0.06	16.78 ± 1e-4	0.612 ± 1e-5	1.583 ± 0.010	0.919 ± 0.004
Male→Female						
CUT [28]	1	31.94	19.87	0.74	-	-
UNSB* [18]	5	28.62	19.55	0.687	0.576	0.635
ILVR [5]	1000	46.12 ± 0.33	18.59 ± 0.02	0.510 ± 0.001	-	-
SDEdit [25]	1000	49.43 ± 0.47	20.03 ± 0.01	0.572 ± 0.000	0.782 ± 0.020	0.380 ± 0.018
EGSDE [46]	1000	41.93 ± 0.11	20.35 ± 0.01	0.574 ± 0.000	0.875 ± 0.032	0.437 ± 0.017
EGSDE† [46]	1200	30.61 ± 0.19	18.32 ± 0.02	0.510 ± 0.001	0.955 ± 0.019	0.621 ± 0.016
SDDM [38]	100	44.37 ± 0.23	-	0.526 ± 0.001	-	-
DDIB* (Teacher) [37]	160	23.69	18.70	0.664	0.969	0.808
IBCD (Ours)	1	24.93 ± 0.03	20.51 ± 4e-4	0.749 ± 3e-5	1.160 ± 0.008	0.814 ± 0.006
IBCD† (Ours)	1	24.70 ± 0.03	20.11 ± 4e-4	0.744 ± 3e-5	1.145 ± 0.003	0.815 ± 0.004

Table 2. **Quantitative comparison of unpaired image-to-image translation tasks.** Most results are from the EGSDE paper, except those marked with *, which are from our re-implementation and Density-Coverage metric [26]. Marker † indicates a hyperparameter configuration prioritizes realism over faithfulness.

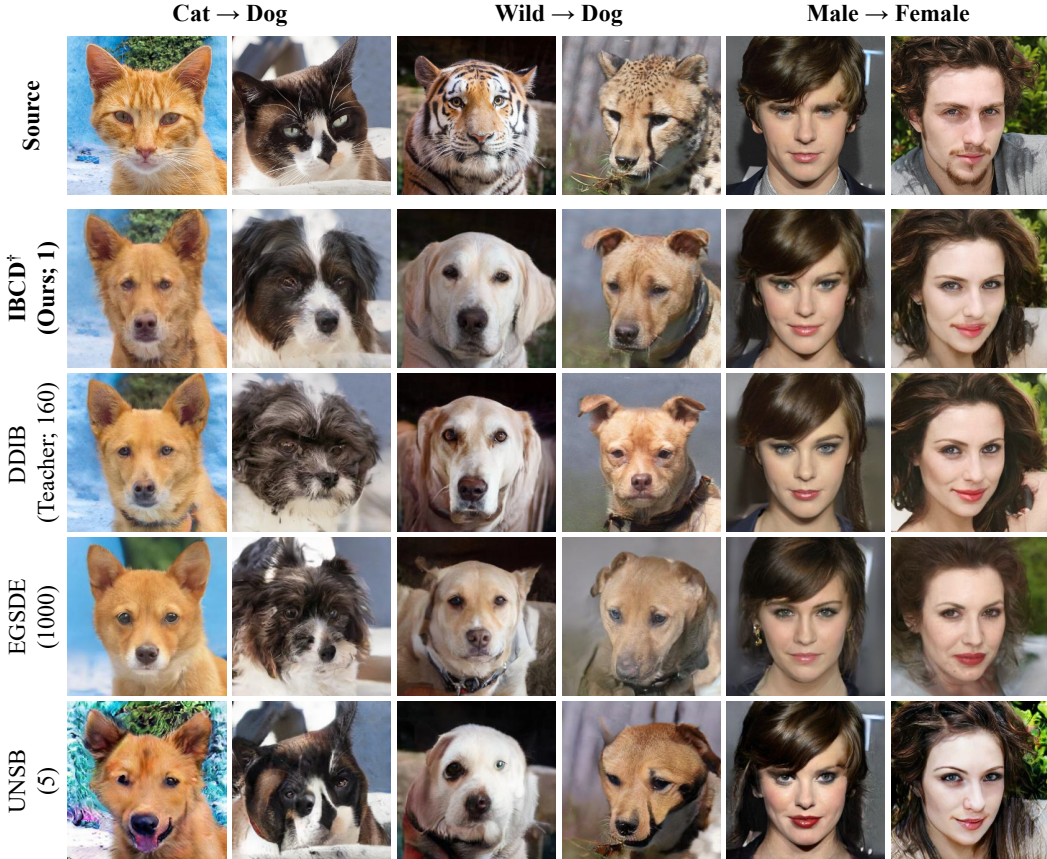


Figure 4. **Qualitative comparison of unpaired image-to-image translation tasks.** Compared to other diffusion-based baselines, our model achieves more realistic and source-faithful translations in a single step. The numbers in parentheses represent inference NFE.

Validity of the IBCD. Fig. 3(a) shows the translation results from domain $A \rightarrow B$ for various models, highlighting the cumulative effectiveness of each component in our framework. Distillation with only the IBCD loss achieves basic translation but incorrectly maps some points to low-density regions of the target domain, particularly from the source domain’s decision boundaries (Appendix D.1). Adding the DMCD loss improves translation by guiding more points toward high-density regions, but it fails to reposition points in low-density areas and reduces mode coverage by pushing points in high-density regions even further. Introducing a cycle loss alleviates the reduction in mode coverage caused by DMCD and refines the decision boundaries in the target domain. Finally, incorporating distillation difficulty adaptive weighting into DMCD selectively corrects points that have drifted into low-density regions, guiding them toward higher-density areas. The complete cycle translation ($A \rightarrow B \rightarrow A$) using a model trained with our final approach effectively demonstrates cycle consistency, validating the robustness and fidelity of our method.

Distillation Difficulty. Fig. 3(b) illustrates the impact of distillation difficulty on the translation process. On the left,

we show the decision boundary of the source domain resulting from the translation from the target to the source domain by the DDIB teacher model. The middle and right panels depict $\mathcal{D}([\mathbf{x}_{t-N+1}, \dots, \mathbf{x}_{t-N-1}], c_b)$ and its expected one-step approximation, $\mathbb{E}_{t \sim \mathcal{U}[-N+1, N-2]}[\hat{\mathcal{D}}(\mathbf{x}_t, c_b)]$ for the $A \rightarrow B$ translation, plotted at the source domain location $\mathbf{x}_{\epsilon(c_a)}$. The distillation difficulty measure effectively captures the decision boundary, indicating challenging regions for the student model. As shown, its one-step approximation provides an accurate and suitable representation of the distillation difficulty, demonstrating its utility in guiding the training process and improving translation accuracy.

4.2. Unpaired Image-to-Image Translation

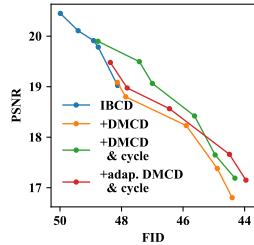
In this section, we apply IBCD to various image-to-image (I2I) translation tasks, which are our primary focus. We comprehensively evaluate its performance across these tasks to demonstrate its effectiveness and robustness.

Evaluation. Following the evaluation methodology and code from EGSDE [46], a widely used benchmark for unpaired I2I tasks, we assessed our approach on the Cat \rightarrow Dog and Wild \rightarrow Dog tasks from the AFHQ dataset [7] and

Table 3. Quantitative ablation study results in the Cat→Dog task *under the lowest FID* (similar FID condition except for the vanilla IBCD).

Component	FID↓	PSNR↑	
		Teacher	Source
IBCD only	48.12	18.27	19.02
+ DMCD	44.40	17.95	16.80
+ DMCD & Cycle	44.31	18.22	17.19
+ adap. DMCD & Cycle	44.69	18.97	18.04

Figure 6. Ablation study results demonstrating improved PSNR-FID trade-off for the Cat→Dog task.



the Male→Female task from the CelebA-HQ dataset [16]. We first trained AFHQ EDM and CelebA-HQ EDM models to serve as teacher models. Single-step Cat↔Dog and Wild↔Dog translation models were distilled from the AFHQ EDM, while the Male↔Female translation model was distilled from the CelebA-HQ EDM. All datasets were resized to 256 pixels for training and evaluation. The metrics used include Fréchet Inception Distance (FID) [13] and Density-Coverage [26] to assess translation realism, and PSNR and SSIM [41] to evaluate the faithfulness of the translation to the original images.

Baselines. As baselines, we compare our method against several GAN-based methods, including CycleGAN [51], Self-Distance [2], GcGAN [9], LeSeSIM [47], StarGAN v2 [7], and CUT [28]. We also benchmark against diffusion model (DM)-based methods such as ILVR [5], SDEdit [25], EGSDE [46], CycleDiffusion [43], and SDDM [38]. Additionally, we compare our approach with UNSB [18], a few-step Schrödinger bridge-based method, and the teacher DDIB [37]. Most of the comparison results are sourced from [46] except for the density-coverage, while the results for UNSB and DDIB are based on our re-implementations.

Comparison results. Fig. 4 and Tab. 2 show that IBCD consistently outperforms baseline models in both qualitative and quantitative comparisons. IBCD strikes a balance between faithfulness and realism, while IBCD[†] emphasizes realism. These results demonstrate our effectiveness in improving the faithfulness-realism trade-off across tasks and metrics. Although the student model shows reduced realism compared to the teacher, it exhibits improved faithfulness. This decline in realism may result from distillation errors, the single-step conversion process, and other factors. Unlike the teacher, the student model integrates information from both domains, possibly leading it to prioritize faithfulness. Interestingly, in some cases, the student’s samples surpass the teacher’s in realism, likely due to auxiliary losses beyond the IBCD loss. This suggests that the student’s ability to combine domain information and auxiliary training components can enhance overall performance.

Ablation Study. We conducted an ablation study on the Cat→Dog task to evaluate the effectiveness of each component. In this study, DMCD loss, cycle translation loss, and

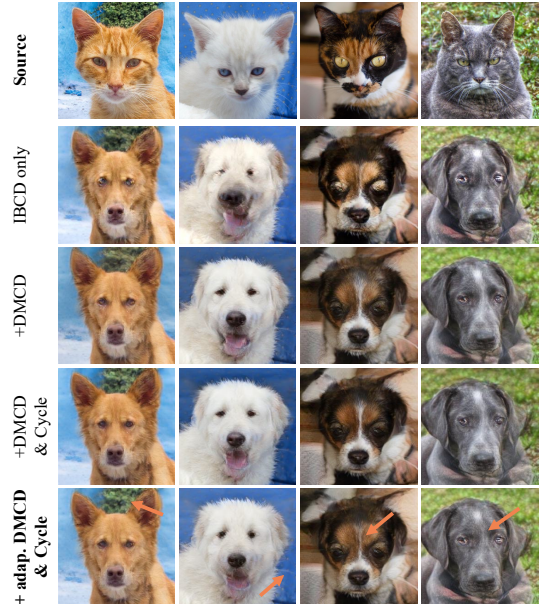


Figure 5. IBCD ablation study results on Cat→Dog task.

distillation difficulty adaptive weighting (adaptive DMCD) were sequentially added to the baseline IBCD loss-only model. To assess distillation error, we calculated PSNR relative to the DDIB teacher (PSNR-teacher), complementing the standard PSNR shown in Tab. 2 (PSNR-source). Fig. 5 and Tab. 3 display the results for each ablated model that achieved the lowest FID. Fig. 6 shows PSNR-FID trade-off curves for various hyperparameters (*e.g.*, λ_{IBCD} , λ_{cycle} , and training steps) for each ablated model. Each component significantly reduces FID beyond the lower bound achieved by vanilla IBCD, while minimizing PSNR degradation due to the task’s inherent trade-off and reducing distillation error. Adaptive DMCD has been particularly effective when prioritizing the lowest FID in the trade-off curve, significantly reducing distillation errors as well. These findings confirm that the components of IBCD work synergistically to improve the balance between faithfulness and realism.

5. Conclusion

In this work, we introduced IBCD, a novel unpaired bidirectional single-step image translation framework. By distilling the diffusion implicit bridge through an extended CD framework, we achieved bidirectional translation without paired data or adversarial training. Our approach overcomes traditional CD limitations with DMCD and distillation difficulty adaptive weighting strategies. Empirical evaluations on toy and high-dimensional datasets demonstrate IBCD’s effectiveness and scalability. We believe IBCD represents a significant advancement in general single-step image translation, offering a versatile and efficient solution for various image tasks, particularly in scenarios with limited paired data and those where low latency is crucial.

References

- [1] Uri M Ascher and Linda R Petzold. *Computer methods for ordinary differential equations and differential-algebraic equations*. SIAM, 1998. 15
- [2] Sagie Benaim and Lior Wolf. One-sided unsupervised domain mapping. *Advances in neural information processing systems*, 30, 2017. 6, 8
- [3] Junhua Chen, Shenlun Chen, Leonard Wee, Andre Dekker, and Inigo Bermejo. Deep learning based unpaired image-to-image translation applications for medical physics: a systematic review. *Physics in Medicine & Biology*, 68(5):05TR01, 2023. 1
- [4] Tianrong Chen, Guan-Horng Liu, and Evangelos A Theodorou. Likelihood training of schrödinger bridge using forward-backward sdes theory. *arXiv preprint arXiv:2110.11291*, 2021. 1
- [5] Jooyoung Choi, Sungwon Kim, Yonghyun Jeong, Youngjune Gwon, and Sungroh Yoon. Ilvr: Conditioning method for denoising diffusion probabilistic models. in *2021 IEEE International Conference on Computer Vision (ICCV)*, page 2, 2021. 6, 8, 18
- [6] Yunjey Choi, Minje Choi, Munyoung Kim, Jung-Woo Ha, Sunghun Kim, and Jaegul Choo. Stargan: Unified generative adversarial networks for multi-domain image-to-image translation. In *Proceedings of the IEEE conference on computer vision and pattern recognition*, pages 8789–8797, 2018. 1, 2
- [7] Yunjey Choi, Youngjung Uh, Jaejun Yoo, and Jung-Woo Ha. Stargan v2: Diverse image synthesis for multiple domains. In *Proceedings of the IEEE/CVF conference on computer vision and pattern recognition*, pages 8188–8197, 2020. 6, 7, 8, 14, 15, 18, 19
- [8] Bradley Efron. Tweedie’s formula and selection bias. *Journal of the American Statistical Association*, 106(496):1602–1614, 2011. 2
- [9] Huan Fu, Mingming Gong, Chaohui Wang, Kayhan Batmanghelich, Kun Zhang, and Dacheng Tao. Geometry-consistent generative adversarial networks for one-sided unsupervised domain mapping. In *Proceedings of the IEEE/CVF conference on computer vision and pattern recognition*, pages 2427–2436, 2019. 1, 6, 8
- [10] Ian Goodfellow, Jean Pouget-Abadie, Mehdi Mirza, Bing Xu, David Warde-Farley, Sherjil Ozair, Aaron Courville, and Yoshua Bengio. Generative adversarial nets. *Advances in neural information processing systems*, 27, 2014. 3
- [11] Amir Hertz, Ron Mokady, Jay Tenenbaum, Kfir Aberman, Yael Pritch, and Daniel Cohen-Or. Prompt-to-prompt image editing with cross attention control. *arXiv preprint arXiv:2208.01626*, 2022. 1
- [12] Amir Hertz, Kfir Aberman, and Daniel Cohen-Or. Delta denoising score. In *Proceedings of the IEEE/CVF International Conference on Computer Vision*, pages 2328–2337, 2023. 1
- [13] Martin Heusel, Hubert Ramsauer, Thomas Unterthiner, Bernhard Nessler, and Sepp Hochreiter. Gans trained by a two time-scale update rule converge to a local nash equilibrium. *Advances in neural information processing systems*, 30, 2017. 8, 15
- [14] Jonathan Ho, Ajay Jain, and Pieter Abbeel. Denoising diffusion probabilistic models. *Advances in neural information processing systems*, 33:6840–6851, 2020. 2
- [15] Shizuo Kaji and Satoshi Kida. Overview of image-to-image translation by use of deep neural networks: denoising, super-resolution, modality conversion, and reconstruction in medical imaging. *Radiological physics and technology*, 12(3): 235–248, 2019. 1
- [16] Tero Karras. Progressive growing of gans for improved quality, stability, and variation. *International Conference on Learning Representations*, 2018. 8, 14
- [17] Tero Karras, Miika Aittala, Timo Aila, and Samuli Laine. Elucidating the design space of diffusion-based generative models. *Advances in neural information processing systems*, 35:26565–26577, 2022. 2, 4, 13, 14
- [18] Beomsu Kim, Gihyun Kwon, Kwanyoung Kim, and Jong Chul Ye. Unpaired image-to-image translation via neural schrödinger bridge. *International Conference on Learning Representations*, 2024. 2, 5, 6, 8, 18
- [19] Dongjun Kim, Chieh-Hsin Lai, Wei-Hsiang Liao, Naoki Murata, Yuhta Takida, Toshimitsu Uesaka, Yutong He, Yuki Mitsufuji, and Stefano Ermon. Consistency trajectory models: Learning probability flow ode trajectory of diffusion. *International Conference on Learning Representations*, 2024. 4
- [20] Kwanyoung Kim and Jong Chul Ye. Noise2score: tweedie’s approach to self-supervised image denoising without clean images. *Advances in Neural Information Processing Systems*, 34:864–874, 2021. 2
- [21] Taeksoo Kim, Moon-su Cha, Hyunsoo Kim, Jung Kwon Lee, and Jiwon Kim. Learning to discover cross-domain relations with generative adversarial networks. In *International conference on machine learning*, pages 1857–1865. Pmlr, 2017. 1
- [22] Liangchen Li and Jiajun He. Bidirectional consistency models. *arXiv preprint arXiv:2403.18035*, 2024. 4, 5
- [23] Guan-Horng Liu, Tianrong Chen, Oswin So, and Evangelos A Theodorou. Deep generalized schrödinger bridge. *arXiv preprint arXiv:2209.09893*, 2022. 1
- [24] Cheng Lu, Yuhao Zhou, Fan Bao, Jianfei Chen, Chongxuan Li, and Jun Zhu. Dpm-solver: A fast ode solver for diffusion probabilistic model sampling in around 10 steps. *Advances in Neural Information Processing Systems*, 35:5775–5787, 2022. 2
- [25] Chenlin Meng, Yutong He, Yang Song, Jiaming Song, Jiajun Wu, Jun-Yan Zhu, and Stefano Ermon. SDEdit: Guided image synthesis and editing with stochastic differential equations. In *International Conference on Learning Representations*, 2022. 1, 2, 6, 8, 18
- [26] Muhammad Ferjad Naeem, Seong Joon Oh, Youngjung Uh, Yunjey Choi, and Jaejun Yoo. Reliable fidelity and diversity metrics for generative models. In *International Conference on Machine Learning*, pages 7176–7185. PMLR, 2020. 6, 8, 15
- [27] Taesung Park, Alexei A. Efros, Richard Zhang, and Jun-Yan Zhu. Contrastive learning for unpaired image-to-image translation. In *Computer Vision – ECCV 2020*, pages 319–345, Cham, 2020. Springer International Publishing. 1

- [28] Taesung Park, Alexei A Efros, Richard Zhang, and Jun-Yan Zhu. Contrastive learning for unpaired image-to-image translation. In *Computer Vision—ECCV 2020: 16th European Conference, Glasgow, UK, August 23–28, 2020, Proceedings, Part IX 16*, pages 319–345. Springer, 2020. 6, 8, 18
- [29] Gaurav Parmar, Krishna Kumar Singh, Richard Zhang, Yijun Li, Jingwan Lu, and Jun-Yan Zhu. Zero-shot image-to-image translation. In *ACM SIGGRAPH 2023 conference proceedings*, pages 1–11, 2023. 1
- [30] Gaurav Parmar, Taesung Park, Srinivasa Narasimhan, and Jun-Yan Zhu. One-step image translation with text-to-image models. *arXiv preprint arXiv:2403.12036*, 2024. 5
- [31] Muhammad Muneeb Saad, Ruairi O’Reilly, and Mubashir Husain Rehmani. A survey on training challenges in generative adversarial networks for biomedical image analysis. *Artificial Intelligence Review*, 57(2):19, 2024. 1
- [32] Mehran Safayani, Behnaz Mirzapour, Hanieh Aghaebrahimian, Nasrin Salehi, and Hamid Ravae. Unpaired image-to-image translation with content preserving perspective: A review. *arXiv preprint arXiv:2502.08667*, 2025. 1
- [33] Erwin Schrödinger. Sur la théorie relativiste de l’électron et l’interprétation de la mécanique quantique. *Annales de l’institut Henri Poincaré*, 2(4):269–310, 1932. 1
- [34] Karen Simonyan. Very deep convolutional networks for large-scale image recognition. *arXiv preprint arXiv:1409.1556*, 2014. 15
- [35] Yang Song, Jascha Sohl-Dickstein, Diederik P Kingma, Abhishek Kumar, Stefano Ermon, and Ben Poole. Score-based generative modeling through stochastic differential equations. In *International Conference on Learning Representations*, 2021. 2
- [36] Yang Song, Prafulla Dhariwal, Mark Chen, and Ilya Sutskever. Consistency models. In *International Conference on Machine Learning*, pages 32211–32252. PMLR, 2023. 2, 3, 13, 14
- [37] Xuan Su, Jiaming Song, Chenlin Meng, and Stefano Ermon. Dual diffusion implicit bridges for image-to-image translation. In *International Conference on Learning Representations*, 2023. 1, 2, 4, 6, 8, 18, 19
- [38] Shikun Sun, Longhui Wei, Junliang Xing, Jia Jia, and Qi Tian. Sddm: score-decomposed diffusion models on manifolds for unpaired image-to-image translation. In *International Conference on Machine Learning*, pages 33115–33134. PMLR, 2023. 1, 6, 8
- [39] Pascal Vincent. A connection between score matching and denoising autoencoders. *Neural computation*, 23(7):1661–1674, 2011. 2
- [40] Gefei Wang, Yuling Jiao, Qian Xu, Yang Wang, and Can Yang. Deep generative learning via schrödinger bridge. In *International Conference on Machine Learning*, pages 10794–10804. PMLR, 2021. 1
- [41] Zhou Wang, Alan C Bovik, Hamid R Sheikh, and Eero P Simoncelli. Image quality assessment: from error visibility to structural similarity. *IEEE transactions on image processing*, 13(4):600–612, 2004. 8
- [42] Zhengyi Wang, Cheng Lu, Yikai Wang, Fan Bao, Chongxuan Li, Hang Su, and Jun Zhu. Prolificdreamer: High-fidelity and diverse text-to-3d generation with variational score distillation. *Advances in Neural Information Processing Systems*, 36:8406–8441, 2023. 3
- [43] Chen Henry Wu and Fernando De la Torre. A latent space of stochastic diffusion models for zero-shot image editing and guidance. In *Proceedings of the IEEE/CVF International Conference on Computer Vision*, pages 7378–7387, 2023. 1, 2, 6, 8, 18, 19
- [44] Tianwei Yin, Michaël Gharbi, Richard Zhang, Eli Shechtman, Fredo Durand, William T Freeman, and Taesung Park. One-step diffusion with distribution matching distillation. In *Proceedings of the IEEE/CVF Conference on Computer Vision and Pattern Recognition*, pages 6613–6623, 2024. 3, 15
- [45] Richard Zhang, Phillip Isola, Alexei A Efros, Eli Shechtman, and Oliver Wang. The unreasonable effectiveness of deep features as a perceptual metric. In *Proceedings of the IEEE conference on computer vision and pattern recognition*, pages 586–595, 2018. 14
- [46] Min Zhao, Fan Bao, Chongxuan Li, and Jun Zhu. Egsde: Unpaired image-to-image translation via energy-guided stochastic differential equations. *Advances in Neural Information Processing Systems*, 35:3609–3623, 2022. 1, 2, 5, 6, 7, 8, 15, 18
- [47] Chuanxia Zheng, Tat-Jen Cham, and Jianfei Cai. The spatially-correlative loss for various image translation tasks. In *Proceedings of the IEEE/CVF conference on computer vision and pattern recognition*, pages 16407–16417, 2021. 6, 8
- [48] Wanfeng Zheng, Qiang Li, Guoxin Zhang, Pengfei Wan, and Zhongyuan Wang. Itr: Unpaired image-to-image translation with transformers. *arXiv preprint arXiv:2203.16015*, 2022. 1
- [49] Linqi Zhou, Aaron Lou, Samar Khanna, and Stefano Ermon. Denoising diffusion bridge models. In *The Twelfth International Conference on Learning Representations*, 2024. 2
- [50] Jun-Yan Zhu, Taesung Park, Phillip Isola, and Alexei A. Efros. Unpaired image-to-image translation using cycle-consistent adversarial networks. In *Proceedings of the IEEE International Conference on Computer Vision (ICCV)*, 2017. 1
- [51] Jun-Yan Zhu, Taesung Park, Phillip Isola, and Alexei A Efros. Unpaired image-to-image translation using cycle-consistent adversarial networks. In *Proceedings of the IEEE international conference on computer vision*, pages 2223–2232, 2017. 2, 5, 6, 8

Single-Step Bidirectional Unpaired Image Translation Using Implicit Bridge Consistency Distillation

Supplementary Material

A. Algorithms

In this section, we present the vanilla implicit bridge consistency distillation algorithm (Algo. 1), which utilizes only the IBCD losses. Additionally, we introduce the final implicit bridge consistency distillation algorithm (Algo. 2), which incorporates all the losses discussed in the text, including DMCD and adaptive weighting strategies, to enhance performance and address the limitations identified in the vanilla version.

Algorithm 1: (Vanilla) Implicit Bridge Consistent Distillation (IBCD)

Input: Teacher diffusion model ϕ , datasets \mathcal{S}_A and \mathcal{S}_B , class conditions c_a and c_b .

```

1  $j \leftarrow 0, \theta \leftarrow \phi, \theta^- \leftarrow \phi$ 
2 repeat
3    $c \leftarrow \text{if } (j \% 2 == 0 \text{ then } c_a \text{ else } c_b)$ 
4   Sample  $\mathbf{x}^a \sim \mathcal{S}_A, \mathbf{x}^b \sim \mathcal{S}_B$ 
5   if  $c == c_b$  then
6     Sample  $n_a \sim \mathcal{U}[-N + 1, -1], n_b \sim \mathcal{U}[0, N - 2]$ 
7   else
8     Sample  $n_a \sim \mathcal{U}[-N + 2, 0], n_b \sim \mathcal{U}[1, N - 1]$ 
9   Sample  $\mathbf{x}_{t_{n_a}} \sim \mathcal{N}(\mathbf{x}^a, t_{n_a}^2 \mathbf{I}), \mathbf{x}_{t_{n_b}} \sim \mathcal{N}(\mathbf{x}^b, t_{n_b}^2 \mathbf{I})$ 
10  if  $c == c_b$  then
11    Estimate  $\hat{\mathbf{x}}_{t_{n_a+1}}, \hat{\mathbf{x}}_{t_{n_b+1}}$  with Eq. (7)
12  else
13    Estimate  $\hat{\mathbf{x}}_{t_{n_a-1}}, \hat{\mathbf{x}}_{t_{n_b-1}}$  with Eq. (8)
14   $\mathbf{t}_1 \leftarrow [t_{n_a}; t_{n_b}], \mathbf{t}_2 = [t_{n_a \pm 1}; t_{n_b \pm 1}]$ 
15   $\mathbf{x}_{\mathbf{t}_1} \leftarrow [\mathbf{x}_{t_{n_a}}; \mathbf{x}_{t_{n_b}}], \hat{\mathbf{x}}_{\mathbf{t}_2} \leftarrow [\hat{\mathbf{x}}_{t_{n_a \pm 1}}; \hat{\mathbf{x}}_{t_{n_b \pm 1}}]$ 
16   $\mathcal{L}_{\text{IBCD}} \leftarrow [\lambda(\mathbf{t}_2) d_{\text{IBCD}}(f_{\theta}(\mathbf{x}_{\mathbf{t}_1}, \mathbf{t}_1, c), f_{\theta^-}(\hat{\mathbf{x}}_{\mathbf{t}_2}, \mathbf{t}_2, c))]$ 
17   $\theta \leftarrow \theta - \zeta_{\theta} \nabla_{\theta} \mathcal{L}_{\text{IBCD}}$ 
18   $\theta^- \leftarrow \text{sg}(\mu \theta^- + (1 - \mu)\theta)$ 
19   $j \leftarrow j + 1$ 

```

20 **until** $\mathcal{L}_{\text{IBCD}}$ convergence;

Output: Unified single-step model f_{θ} for bidirectional image translation.

Algorithm 2: (Final) Implicit Bridge Consistent Distillation (IBCD)

Input: Teacher diffusion model ϕ , datasets \mathcal{S}_A and \mathcal{S}_B , class conditions c_a and c_b .

```
1  $j \leftarrow 0, \theta \leftarrow \phi, \theta^- \leftarrow \phi, \psi \leftarrow \phi$ 
2 repeat
3    $c \leftarrow \text{if } (j \% 2 == 0 \text{ then } c_a \text{ else } c_b)$ 
4   Sample  $\mathbf{x}^a \sim \mathcal{S}_A, \mathbf{x}^b \sim \mathcal{S}_B$ 
   //
   // IBCD loss
5   if  $c == c_b$  then
6     Sample  $n_a \sim \mathcal{U}[-N + 1, -1], n_b \sim \mathcal{U}[0, N - 2]$ 
7   else
8     Sample  $n_a \sim \mathcal{U}[-N + 2, 0], n_b \sim \mathcal{U}[1, N - 1]$ 
9   Sample  $\mathbf{x}_{t_{n_a}} \sim \mathcal{N}(\mathbf{x}^a, t_{n_a}^2 \mathbf{I}), \mathbf{x}_{t_{n_b}} \sim \mathcal{N}(\mathbf{x}^b, t_{n_b}^2 \mathbf{I})$ 
10  if  $c == c_b$  then
11    Estimate  $\hat{\mathbf{x}}_{t_{n_a+1}}, \hat{\mathbf{x}}_{t_{n_b+1}}$  with Eq. (7)
12  else
13    Estimate  $\hat{\mathbf{x}}_{t_{n_a-1}}, \hat{\mathbf{x}}_{t_{n_b-1}}$  with Eq. (8)
14   $\mathbf{t}_1 \leftarrow [t_{n_a}; t_{n_b}], \mathbf{t}_2 = [t_{n_a \pm 1}; t_{n_b \pm 1}]$ 
15   $\mathbf{x}_{\mathbf{t}_1} \leftarrow [\mathbf{x}_{t_{n_a}}; \mathbf{x}_{t_{n_b}}], \hat{\mathbf{x}}_{\mathbf{t}_2} \leftarrow [\hat{\mathbf{x}}_{t_{n_a \pm 1}}; \hat{\mathbf{x}}_{t_{n_b \pm 1}}]$ 
16   $\mathcal{L}_{\text{IBCD}} \leftarrow [\lambda(\mathbf{t}_2) d_{\text{IBCD}}(f_\theta(\mathbf{x}_{\mathbf{t}_1}, \mathbf{t}_1, c), f_{\theta^-}(\hat{\mathbf{x}}_{\mathbf{t}_2}, \mathbf{t}_2, c))]$ 
   //
   // DMCD loss
17  Sample  $i \sim \mathcal{U}[0, N - 1]$ 
18  Sample  $\mathbf{x}_{t_i} \sim \mathcal{N}(f_\theta(\mathbf{x}_{\mathbf{t}_1}, \mathbf{t}_1, c), t_i^2 \mathbf{I})$ 
19   $\hat{D} \leftarrow \text{sg}(g(d_{\text{DMCD}}(f_\theta(\mathbf{x}_{\mathbf{t}_1}, \mathbf{t}_1, c), f_{\theta^-}(\hat{\mathbf{x}}_{\mathbf{t}_2}, \mathbf{t}_2, c))))$ 
20   $\nabla_\theta \mathcal{L}_{\text{DMCD}} \leftarrow w_{t_i} \hat{D} \cdot (s_\psi(\mathbf{x}_{t_i}, t_i, c) - s_\phi(\mathbf{x}_{t_i}, t_i, c)) \nabla_\theta f_\theta(\mathbf{x}_{\mathbf{t}_1}, \mathbf{t}_1, c)$ 
   //
   // Cycle loss
21  Sample  $\mathbf{x}_{\epsilon(c_a)} \sim \mathcal{N}(\mathbf{x}^a, \sigma_{\min}^2 \mathbf{I}), \mathbf{x}_{\epsilon(c_b)} \sim \mathcal{N}(\mathbf{x}^b, \sigma_{\min}^2 \mathbf{I})$ 
22   $\mathbf{t}_3 \leftarrow [\epsilon(c_a); \epsilon(c_b)], \mathbf{t}_4 \leftarrow [\epsilon(c_b); \epsilon(c_a)]$ 
23   $\mathbf{c}_3 \leftarrow [c_b; c_a], \mathbf{c}_4 \leftarrow [c_a; c_b]$ 
24   $\mathbf{x}_{\mathbf{t}_3} \leftarrow [\mathbf{x}_{\epsilon(c_a)}; \mathbf{x}_{\epsilon(c_b)}]$ 
25   $\mathcal{L}_{\text{cycle}} \leftarrow d_{\text{cycle}}(f_\theta(f_\theta(\mathbf{x}_{\mathbf{t}_3}, \mathbf{t}_3, \mathbf{c}_3), \mathbf{t}_4, \mathbf{c}_4), \mathbf{x}_{\mathbf{t}_3})$ 
   //
   // Optimize the student
26   $\nabla_\theta \mathcal{L}_{\text{total}} \leftarrow \nabla_\theta \mathcal{L}_{\text{IBCD}} + \lambda_{\text{DMCD}} \nabla_\theta \mathcal{L}_{\text{DMCD}} + \lambda_{\text{cycle}} \nabla_\theta \mathcal{L}_{\text{cycle}}$ 
27   $\theta \leftarrow \theta - \zeta_\theta \nabla_\theta \mathcal{L}_{\text{total}}$ 
28   $\theta^- \leftarrow \text{sg}(\mu \theta^- + (1 - \mu) \theta)$ 
   //
   // Optimize the fake DM
29   $\mathcal{L}_{\text{DSM}} \leftarrow \text{DSM loss of EDM with sample } f_\theta(\mathbf{x}_{\mathbf{t}_1}, \mathbf{t}_1, c), \text{ class condition } c, \text{ and fake DM } \phi$ 
30   $\phi \leftarrow \phi - \zeta_\phi \nabla_\phi \mathcal{L}_{\text{DSM}}$ 
31   $j \leftarrow j + 1$ 
32 until  $\mathcal{L}_{\text{total}}$  convergence;
Output: Unified single-step model  $f_\theta$  for bidirectional image translation.
```

B. Extending EDM/CD for the IBCD

Model Parametrization. The EDM [17] parametrization for the student f_θ in consistency distillation [36] is defined as follows for positive real-valued t and the neural network F_θ :

$$f_\theta(\mathbf{x}_t, t) = c_{\text{skip}}(t)\mathbf{x}_t + c_{\text{out}}(t)F_\theta(c_{\text{in}}(t)\mathbf{x}_t, t'(t)). \quad (14)$$

In CD, authors choose

$$c_{\text{skip}}(t) = \frac{\sigma_{\text{data}}^2}{(t - \epsilon)^2 + \sigma_{\text{data}}^2}, \quad c_{\text{out}}(t) = \frac{\sigma_{\text{data}}(t - \epsilon)}{\sqrt{\sigma_{\text{data}}^2 + t^2}}, \quad c_{\text{in}}(t) = \frac{1}{\sqrt{\sigma_{\text{data}}^2 + t^2}}, \quad (15)$$

$$t'(t) = 250 \cdot \ln(t + 10^{-44}) \quad (16)$$

to satisfies the boundary condition $f(\mathbf{x}_\epsilon, \epsilon) = \mathbf{x}_\epsilon$, and rescales the timestep.

For IBCD, we parametrize the student f_θ for non-zero real-valued t and target domain condition c as:

$$f_\theta(\mathbf{x}_t, t, c) = c_{\text{skip}}(t, c)\mathbf{x}_t + c_{\text{out}}(t, c)F_\theta(c_{\text{in}}(t, c)\mathbf{x}_t, t'(t)), \quad (17)$$

which reflects the necessity for c_{skip} , c_{out} , and c_{in} depend on target domain condition c , ensuring that the proper boundary conditions can be applied at $t = \epsilon(c)$ depending on the target domain $c \in \{c_a, c_b\}$ direction.

Although the student model is fully trained during the distillation process and does not theoretically need to be compatible with the teacher model, initializing it using the teacher model makes it advantageous to design the student to be as compatible as possible. We select c_{skip} , c_{out} , and c_{in} according to Eq. (18), (19), (20), ensuring continuity and compliance with the new boundary conditions while maintaining the definitions within the target domain regions ($t > 0$ for $c = c_b$, $t < 0$ for $c = c_a$).

$$c_{\text{skip}}(t, c) = \begin{cases} \frac{1 + \text{sign}(t)}{2} \frac{\sigma_{\text{data}}^2}{(t - \epsilon(c))^2 + \sigma_{\text{data}}^2} & \text{if } c = c_b \\ \frac{1 + \text{sign}(-t)}{2} \frac{\sigma_{\text{data}}^2}{(t - \epsilon(c))^2 + \sigma_{\text{data}}^2} & \text{if } c = c_a \end{cases} \quad (18)$$

$$c_{\text{out}}(t, c) = \begin{cases} \frac{1 + \text{sign}(t)}{2} \frac{\sigma_{\text{data}}(t - \epsilon(c))}{\sqrt{\sigma_{\text{data}}^2 + t^2}} + \frac{1 - \text{sign}(t)}{2} \sigma_{\text{data}} & \text{if } c = c_b \\ -\frac{1 + \text{sign}(-t)}{2} \frac{\sigma_{\text{data}}(t - \epsilon(c))}{\sqrt{\sigma_{\text{data}}^2 + t^2}} + \frac{1 - \text{sign}(-t)}{2} \sigma_{\text{data}} & \text{if } c = c_a \end{cases} \quad (19)$$

$$c_{\text{in}}(t, c) = \frac{1}{\sqrt{\sigma_{\text{data}}^2 + t^2}} \quad (20)$$

We also extend the timestep rescaler as Eq. (21) to a symmetric and continuous form, ensuring shape compatibility with the original positive-bound domain. This symmetric design reflects the fact that the sign of the timestep separates the domains, while its absolute value represents the noise magnitude:

$$t'(t) = 250 \cdot \text{sign}(t)(\ln(|t| + 10^{-3}) - \ln(\sigma_{\text{max}} + 10^{-44})). \quad (21)$$

This approach preserves the structural integrity of the model and maintains consistent behavior across both domains. The parametrization extension of EDM/CD, as presented here, is visually illustrated in Fig. 7.

Non-differentiability of the ODE Path. In this paragraph, we address the behavior of IBCD at the continuous but non-differentiable point at the center of the PF-ODE trajectory ($i = 0$). Despite the introduction of this point, we show that Theorem 1 from [36] (Appendix A.2) remains applicable, thereby proving the validity of the consistency distillation framework. First, the Lipschitz condition for $f_\theta(x_t, t)$ continues to hold. The primary distinction between IBCD and CD occurs in the t direction, and so we focus on this aspect. The output of f_θ , which predicts the clean target domain image, remains constant along a given PF-ODE trajectory, independent of t . As a result, the Lipschitz condition is not impacted by the non-differentiable point, as the trajectory is continuous. Since the change in the x_t direction is equivalent to that in the CD framework, the Lipschitz continuity assumption from CD is still valid.

Next, we consider the local truncation error of the ODE solver. The non-differentiable point is appropriately captured by our discretization scheme. At this point, the gradient is a combination of gradients from both sides of the trajectory, ensuring stable numerical integration. For example, using an Euler solver in the forward direction (from domain A to domain B):

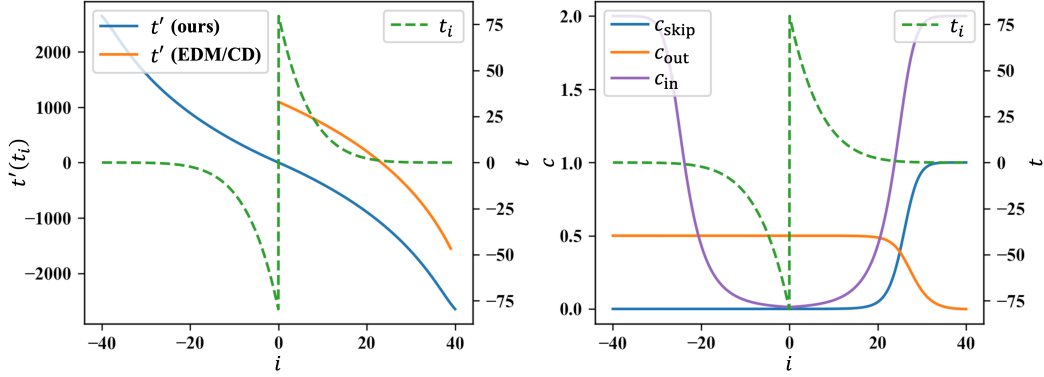


Figure 7. **Extension of EDM/CD model formulation for negative t in IBCD student model.** c_{skip} , c_{out} , and c_{in} represent when $c = c_b$ (the translation direction is $\mathcal{X}_A \rightarrow \mathcal{X}_B$).

- The interval $i = [-1, 0]$ uses the gradient at -1 (from domain A).
- The interval $i = [0, 1]$ uses the gradient at 0 (from domain B).

In the backward direction (from domain B to domain A):

- The interval $i = [0, 1]$ uses the gradient at 1 (from domain B).
- The interval $i = [-1, 0]$ uses the gradient at 0 (from domain A).

Thus, due to the properties of the consistency function and the careful treatment of the non-differentiable point, the error bound of the consistency function remains $O((\Delta t)^p)$, consistent with the original CD approach. The validity of the Lipschitz condition and the equivalence of the local truncation error in the ODE solver ensure that the theorem holds true within the IBCD framework.

C. Implementation Details

Model Architectures. All models used in this study – the teacher ϕ , student θ , and fake DM ψ – employed the same model architecture as in EDM/CD [17, 36]. The architecture configuration followed that of the LSUN-256 teacher EDM model introduced by Song et al. [36]. However, the student model was further modified with the model parametrization described in Appendix B, while the teacher and fake DM maintained the original EDM parametrization.

Teacher Model Training. The teacher model was trained using the EDM implementation and the LSUN-256 model training configuration provided by Song et al. [36]. The training setup included a log-normal schedule sampler and L2 loss, with a global batch size of 288, a learning rate of $1e-4$, a dropout rate of 0.1, and an exponential moving average (EMA) of 0.9999. Mixed precision training was enabled, and weight decay was not applied. The teacher model was trained with class conditions on two types of AFHQ-256 models (cat, dog, and wild) and CelebA-HQ-256 models (female and male). The AFHQ and CelebA-HQ models were trained using their respective training sets from the AFHQ [7] and CelebA-HQ [16] datasets. Each model was trained for approximately 5 days, completing 800K steps on an NVIDIA A100 40GB eight GPU setup.

Implicit Bridge Consistency Distillation. The discretization of DDIB trajectories is defined by extending the sampling discretization of EDM to satisfy Eq. (5):

$$t_i = \sigma_i = \begin{cases} \text{sign}(i)(\sigma_{\max}^{1/\rho} + \frac{|i|}{N-1}(\sigma_{\min}^{1/\rho} - \sigma_{\max}^{1/\rho}))^\rho & (N < i < N) \\ 0 & (i = \pm N) \end{cases} \quad (22)$$

$$\text{where } \text{sign}(x) = \begin{cases} +1 & (x \geq 0) \\ -1 & (x < 0) \end{cases}, \sigma_{\min} = 0.002, \sigma_{\max} = 80, \sigma_{\text{data}} = 0.5, N = 40, \rho = 7.0.$$

For the distance function d in each loss, d_{IBCD} and d_{DMCD} were based on LPIPS [45], while d_{cycle} used the L1 loss. The EMA parameter of the EMA model θ^- was 0.95, and an additional EMA with a separate parameter 0.9999432189950708

was applied to the student model θ and used during inference. The global batch size was 256, with the student learning rate of $4e-5$ and the fake DM learning rate of $1e-4$. Dropout and weight decay were not used, and mixed precision learning was employed.

The ODE solver used was the 2nd order Huen solver [1], consistent with EDM/CD. The weight scheduler for the IBCD loss employed $\lambda(t) = 1$, while the DMCD loss used the weight scheduler w_t as suggested in Yin et al. [44]. For the three tasks, Cat \leftrightarrow Dog, Wild \leftrightarrow Dog models were distilled using the AFHQ-256 teacher model and its corresponding training dataset. The Male \leftrightarrow Female models were distilled using the CelebA-HQ-256 teacher model and its training dataset.

The distillation process began with only the IBCD loss and transitioned to using the full loss set once the FID [13] evaluation metrics stabilized (*i.e.* transition step). Distillation was conducted on the same NVIDIA A100 40GB eight hardware used for training the teacher model. Additional hyperparameters for each model and configuration are detailed in Tab. 4.

Evaluation. We followed the evaluation methodology and tasks outlined in EGSDE [46]. The publicly available evaluation code² was used without modification. Validation sets from the AFHQ and CelebA-HQ datasets were used as the evaluation datasets. All images in each validation set were translated using the respective task-specific models. For each image pair (source domain and translated target domain), PSNR and SSIM were computed, and the average values across all pairs were reported.

FID [13] was calculated using the `pytorch-fid`³ library to measure the distance between the real target domain image distribution and the translated target image distribution. Following the methodology of Choi et al. [7] and Zhao et al. [46], images from the CelebA-HQ dataset were resized and normalized before FID calculation, while images for other tasks were evaluated without additional preprocessing. L2 distance measurement was not included in this evaluation.

Density-coverage [26] was computed using `prdc-cls`⁴ between the distribution of real target domain images and the distribution of images translated into the target domain, similar to the FID measurement. The measurement mode was `T4096` (features of the `fc2` layer of the ImageNet pre-trained VGG16 [34] model). The metric was computed for the entire dataset at once, without using mini-batches. Unlike FID, no specific transformation was applied for the CelebA-HQ dataset.

Reproductions. To evaluate our method, we replicated UNSB and DDIB, two approaches that have not been previously evaluated on our benchmark datasets. For UNSB, we used the publicly available official code for both training and inference, following the default configuration for the Horse \rightarrow Zebra task and training the model for 400 epochs. During inference, we performed 5 steps. For DDIB, we implemented the method within our framework. Specifically, DDIB was executed by first solving the ODE backward from the source domain, then solving it forward again to the target domain using the EDM model trained for IBCD. The ODE solver was implemented in the same manner as the EDM sampler, utilizing the same sampling hyperparameters defined for EDM/IBCD. This setup ensured consistency in the evaluation and allowed for a direct comparison of performance across methods.

We also re-sampled the result from models (CUT, ILVR, SDEdit, EGSDE, CycleDiffusion) for which the density-coverage [26] metric was not originally reported. The density-coverage metric was measured for these models using the method described above and included the results in Tab. 2. The target of measurement for density-coverage was limited to baseline models that met the following criteria: 1) Open-source code and checkpoints were available. 2) FID, PSNR, and SSIM values reported by the authors could be reproduced using the reported sampling strategy. This ensured that all metrics in Tab. 2 were measured on consistent samples.

D. Further Experimental Results

D.1. Distillation Error in Vanilla IBCD

Fig. 8 illustrates the distillation error that arises when using only vanilla IBCD loss on the synthetic toy dataset. When generating samples from pure noise to domain B (Fig. 8 (a)) or translating samples from domain A to domain B (Fig. 8 (b)) using only IBCD loss, the translated results often fall in the low-density region of the target distribution. These translated points primarily originate from the source domain decision boundary, which is the boundary separating the partition in the source domain that should be mapped to two different target domain modes. Translation errors are more pronounced in longer neural jump paths, such as those involved in translations ($i = -N + 1 \rightarrow N - 1$), compared to shorter paths in generation ($i = 0 \rightarrow N - 1$).

²<https://github.com/ML-GSAI/EGSDE>

³<https://github.com/mseitzer/pytorch-fid>

⁴<https://github.com/Mahmood-Hussain/generative-evaluation-prdc>

Table 4. Specific hyperparameters employed by different models and configurations.

Model Configuration	Cat↔Dog		Wild↔Dog		Male↔Female	
	IBCD	IBCD [†]	IBCD	IBCD [†]	IBCD	IBCD [†]
λ_{DMCD}	1	0.18	0.2	0.2	0.02	0.02
λ_{cycle}	0.03	0.003	0.001	0.0003	0.00001	0.00003
$g(\cdot)$	1		min(log(\cdot) + 10)			
transition step	200K	200K	200K	200k	500K	500K
total distillation step	210K	230K	210K	230K	510K	520K

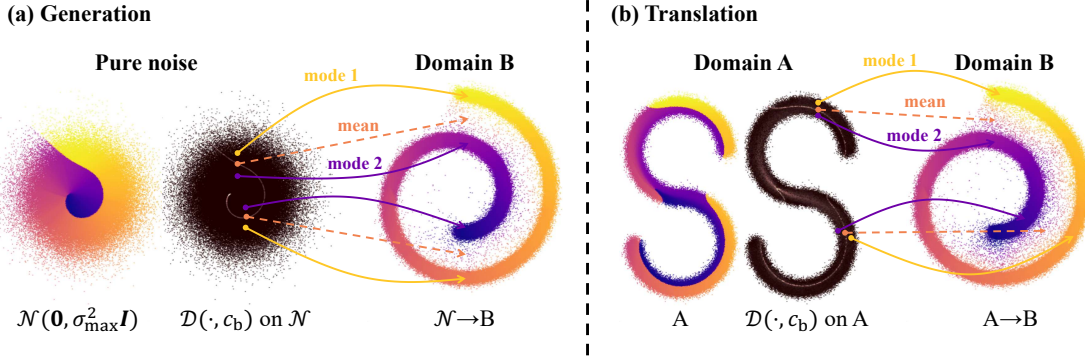


Figure 8. **Incorrect mapping to low-density regions due to the distillation error.** (a) Generation with vanilla IBCD and (b) translation with vanilla IBCD.

D.2. Effect of the Auxiliary Loss Weights

Following the component ablation study of IBCD in the main text, we further investigated the influence of auxiliary loss weights on translation outcomes. Specifically, we varied the weight of the DMCD loss λ_{DMCD} and the cycle loss λ_{cycle} in the Male→Female task (Fig. 9). During these experiments, distillation difficulty adaptive weighting was not applied. The results aligned with expectations: as λ_{DMCD} increases, the realism of the translation result improved, while increasing λ_{cycle} enhanced the faithfulness of the translation. Thus, in the realism-faithfulness trade-off curve, the DMCD loss emphasizes realism, whereas the cycle loss emphasizes faithfulness.

D.3. Approximated Distillation Difficulty in Image-to-image Translation

To explore the implications of the approximated distillation difficulty for real image-to-image translation tasks, we computed an expected approximated distillation difficulty $\mathbb{E}_{t \sim \mathcal{U}[-N+1, N-2]}[\hat{\mathcal{D}}(\mathbf{x}_t, c_{\text{FEMALE}})]$ for all trajectories generated with the DDIB teacher in the Male→Female task using the vanilla IBCD model. We then selected the trajectories with the top 10 and bottom 10 approximate distillation difficulties and performed Male→Female translation using the vanilla IBCD model for these trajectories, as shown in Fig. 10 without cherry-picking. The results indicate that the IBCD model struggles to effectively transform source images from trajectories with high approximate distillation difficulty into target images compared to those with low approximate distillation difficulty. Specifically, the translation results within the top 10 distillation difficulty group exhibit relatively inferior image quality, highlighting the impact of distillation difficulty on translation performance.

D.4. Model Inference Efficiency

To reflect real-world constraints such as model size and inference algorithms, we conducted an inference speed comparison experiment. Instead of relying solely on NFE comparisons, we measured the actual inference time for a Cat→Dog task on a single NVIDIA GeForce RTX 4090 GPU. Tab. 5 presents the average inference time per image and the relative time for each methodology. The batch size was set to maximize GPU VRAM utilization (24 GB), and if the official code did not support parallel sampling, a batch size of 1 was used. The results demonstrate that our methodology is the most computationally efficient even in real-world sampling scenarios.

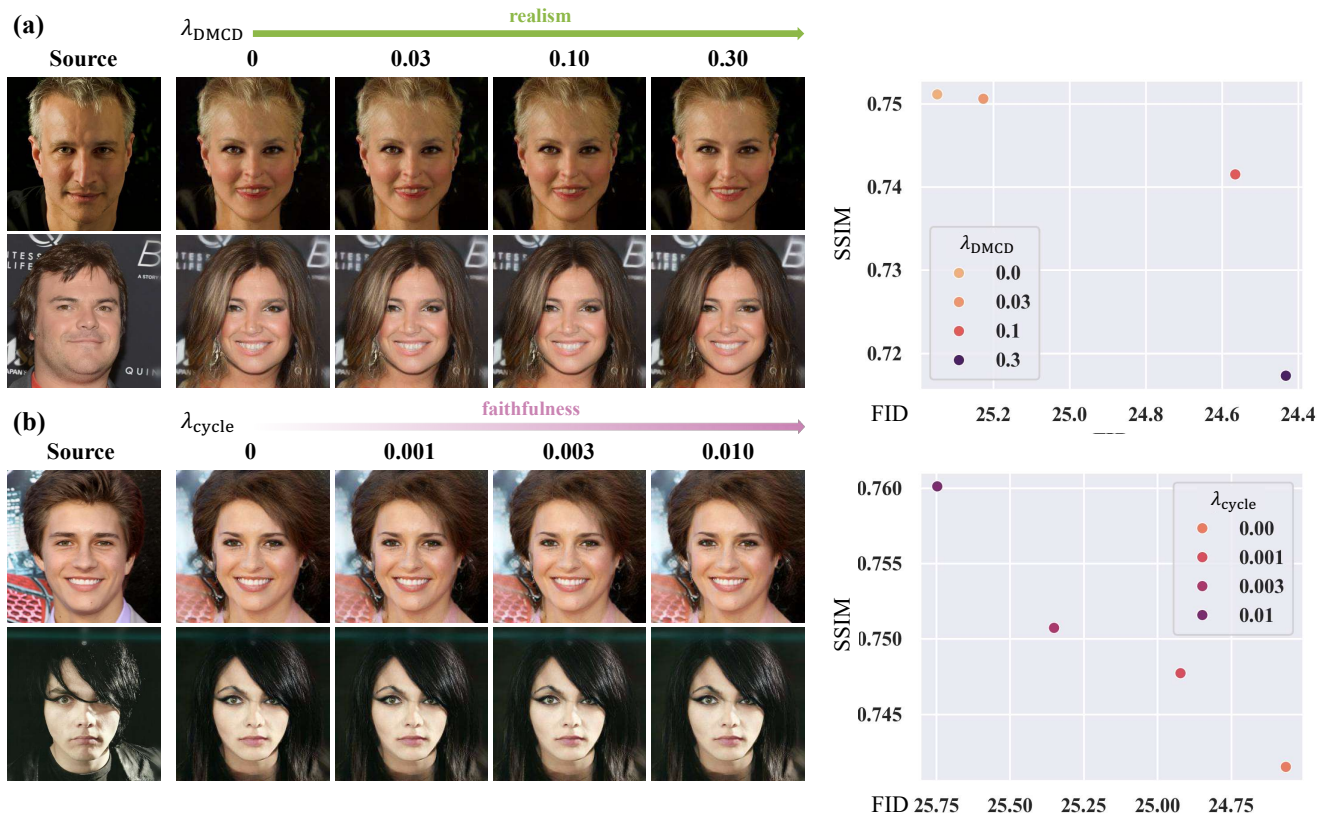


Figure 9. Effect of the auxiliary loss weights (λ_{DMCD} , λ_{cycle}) for the Male→Female task. In (a) λ_{cycle} was set to 0, and in (b) λ_{DMCD} was set to 0.10. Distillation difficulty adaptive waiting was not applied.

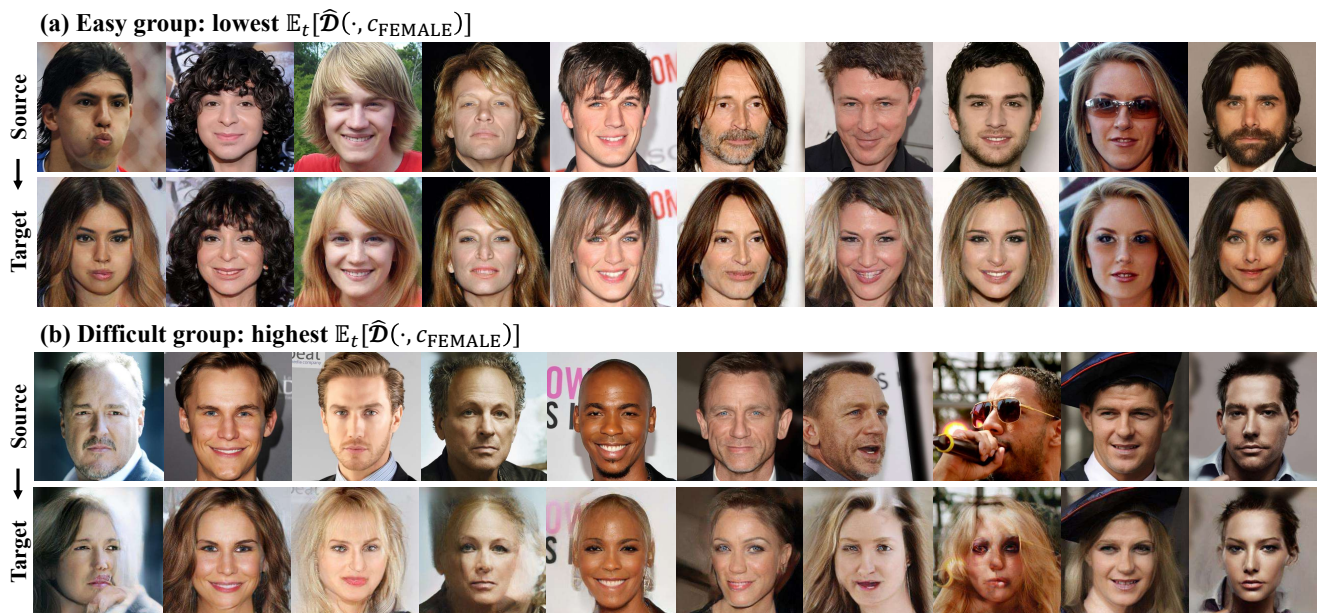


Figure 10. Relationship between self-assessed approximate distillation difficulty $\mathbb{E}_t[\hat{\mathcal{D}}(\cdot, c_{\text{FEMALE}})]$ and the translations performed in the Male→Female task.

Table 5. **Quantitative comparison of model inference times.** *Not supported parallel sampling.

Method	Batch size	NFE ↓	Time [s/img] ↓	Relative Time ↓
StarGAN v2 [7]	256	1	0.058	5.5
CUT [28]	1*	1	0.068	6.4
UNSB [18]	1*	5	0.104	9.9
ILVR [5]	50	1000	12.915	1224.2
SDEdit [25]	70	1000	6.378	604.5
EGSDE [46]	13	1000	15.385	1458.3
CycleDiffusion [43]	1*	1000(+100)	26.032	2467.5
DDIB (Teacher) [37]	165	160	0.956	90.6
IBCD (Ours)	165	1	0.011	1

D.5. Failure Cases

IBCD occasionally produces failure cases as illustrated in Fig. 11. The primary failures can be attributed to incomplete translations (Fig. 11(a)) and incorrect cycle translations (Fig. 11(b)), which are likely due to distillation errors and the side effects of auxiliary losses. Distillation errors from the CD, in particular, appear to be the primary reason. The DMCD and cycle translation loss can also contribute to these issues, with the former leading to incorrect cycle translations and the latter to incomplete translations. Minimizing distillation errors through improved distillation methods and advanced weighting strategies for auxiliary losses might address this issue.

D.6. Bidirectional Translations

To evaluate IBCD’s bidirectional translation capabilities, we compared it to baseline methods through two tasks: *opposite translation* and *cycle translation*. Opposite translation involves reversing the main translation task (Dog→Cat, Dog→Wild, Female→Male), while cycle translation involves performing the reverse task after the main translation (Cat→Dog→Cat, Wild→Dog→Wild, Male→Female→Male). To ensure a fair comparison of bidirectional performance, we used the same model and sampling hyperparameters for each domain pair (Cat↔Dog, Wild↔Dog, Male↔Female) in both opposite and cycle translation tasks.

Given the limited number of models capable of bidirectional translation, we selected StarGAN v2 [7], CycleDiffusion [43], and DDIB (teacher) [37] as baselines. We measured FID for the final target domain for the cycle translation task. It’s worth noting that StarGAN v2’s inference process differs from its main translation task (Tab. 2) performed by Zhao et al. [46] for a better fair comparison. It inputs the same source image as both the source and reference images, enabling it to achieve both high realism and faithfulness.

Tab. 6 and Fig. 12, 13 demonstrate that our model also excels in reverse and cycle translation tasks, exhibiting the best performance and high efficiency. This further supports its strong bidirectional translation capabilities.

D.7. More Qualitative Results

In this section, we present additional qualitative results obtained through cycle translation tasks (Cat→Dog→Cat, Wild→Dog→Wild, Male→Female→Male). The results of the Cat↔Dog, Wild↔Dog, and Male↔Female model are illustrated in Fig. 14, 15, 16. These results highlight our model’s one-way and bidirectional translation capabilities.

Table 6. **Quantitative comparison of unpaired image-to-image translation tasks (opposite & cycle translation).** The opposition task used the same model and inference hyperparameters as the main direction task using bi-directionality.

Method	NFE ↓	FID ↓	PSNR ↑	SSIM ↑	Density ↑	Coverage ↑
Dog→Cat						
StarGAN v2 [7]	1	37.73	16.02	0.399	1.336	0.778
CycleDiffusion [43]	1000(+100)	40.45	17.83	0.493	1.064	0.774
DDIB (Teacher) [37]	160	30.28	17.15	0.597	2.071	0.902
IBCD (Ours)	1	28.99	19.10	0.695	1.699	0.894
IBCD† (Ours)	1	28.41	17.40	0.653	2.112	0.920
Dog→Wild						
StarGAN v2 [7]	1	49.35	16.17	0.386	0.772	0.478
CycleDiffusion [43]	1000(+100)	27.01	16.99	0.421	0.816	0.752
DDIB (Teacher) [37]	160	13.20	16.80	0.583	1.202	0.760
IBCD (Ours)	1	18.79	17.56	0.671	0.900	0.830
IBCD† (Ours)	1	16.67	16.22	0.646	1.058	0.814
Female→Male						
StarGAN v2 [7]	1	59.56	15.75	0.465	1.145	0.587
DDIB (Teacher) [37]	160	26.98	18.74	0.668	1.154	0.858
IBCD (Ours)	1	31.28	19.93	0.733	1.300	0.808
IBCD† (Ours)	1	31.49	19.51	0.726	1.311	0.809
Cat→Dog→Cat						
StarGAN v2 [7]	1	30.53	16.30	0.382	1.717	0.890
CycleDiffusion [43]	1000(+100)	39.59	19.01	0.434	0.731	0.676
DDIB (Teacher) [37]	160	16.56	25.88	0.804	1.330	0.990
IBCD (Ours)	1	22.42	22.35	0.767	1.322	0.992
IBCD† (Ours)	1	24.03	20.28	0.724	1.749	0.988
Wild→Dog→Wild						
StarGAN v2 [7]	1	37.76	15.30	0.285	1.102	0.566
CycleDiffusion [43]	1000(+100)	19.43	16.39	0.281	0.649	0.616
DDIB (Teacher) [37]	160	6.75	26.08	0.803	1.118	0.974
IBCD (Ours)	1	9.89	20.56	0.739	1.118	0.972
IBCD† (Ours)	1	10.66	18.80	0.693	1.259	0.968
Male→Female→Male						
StarGAN v2 [7]	1	57.80	15.39	0.502	1.634	0.728
DDIB (Teacher) [37]	160	28.29	27.70	0.853	0.821	0.993
IBCD (Ours)	1	39.84	22.22	0.790	1.341	0.979
IBCD† (Ours)	1	39.96	21.85	0.783	1.332	0.984

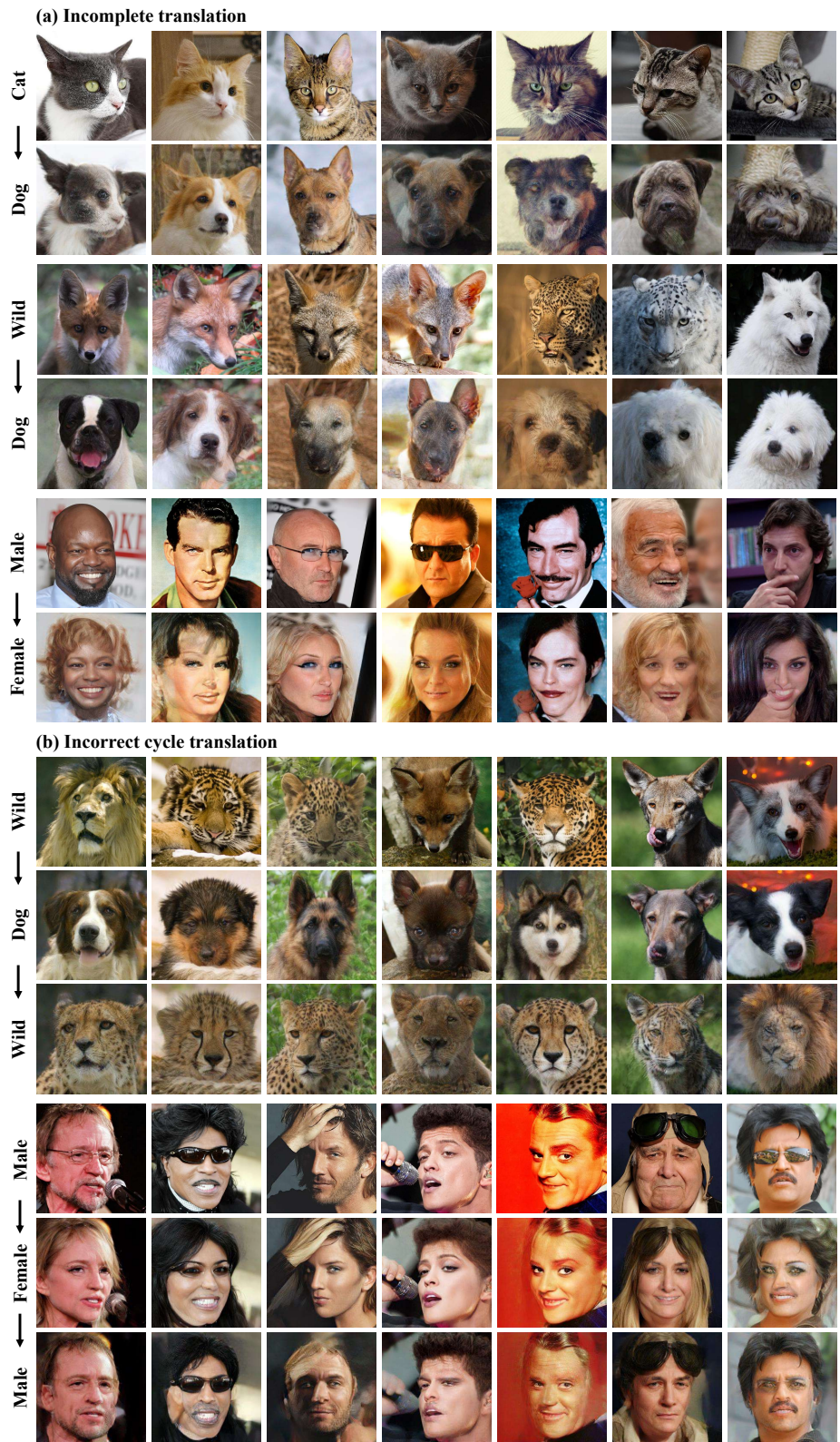


Figure 11. Example of failure cases, which are (a) incomplete translation and (b) incorrect cycle translation.

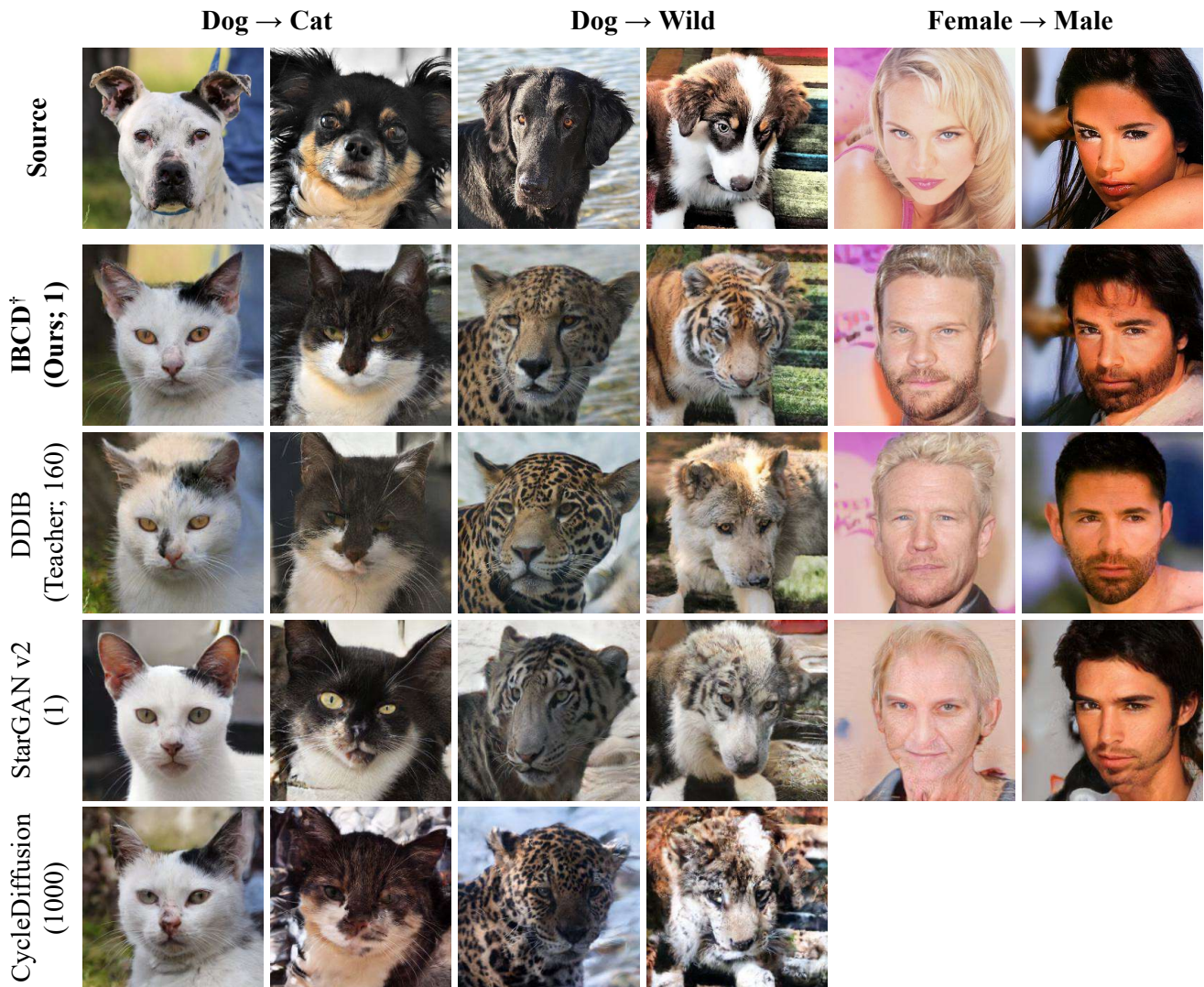


Figure 12. **Qualitative comparison of unpaired image-to-image translation tasks (opposite translation).** Compared to other baselines, our model achieves more realistic and source-faithful translations in a single step. The numbers in parentheses represent inference NFE.

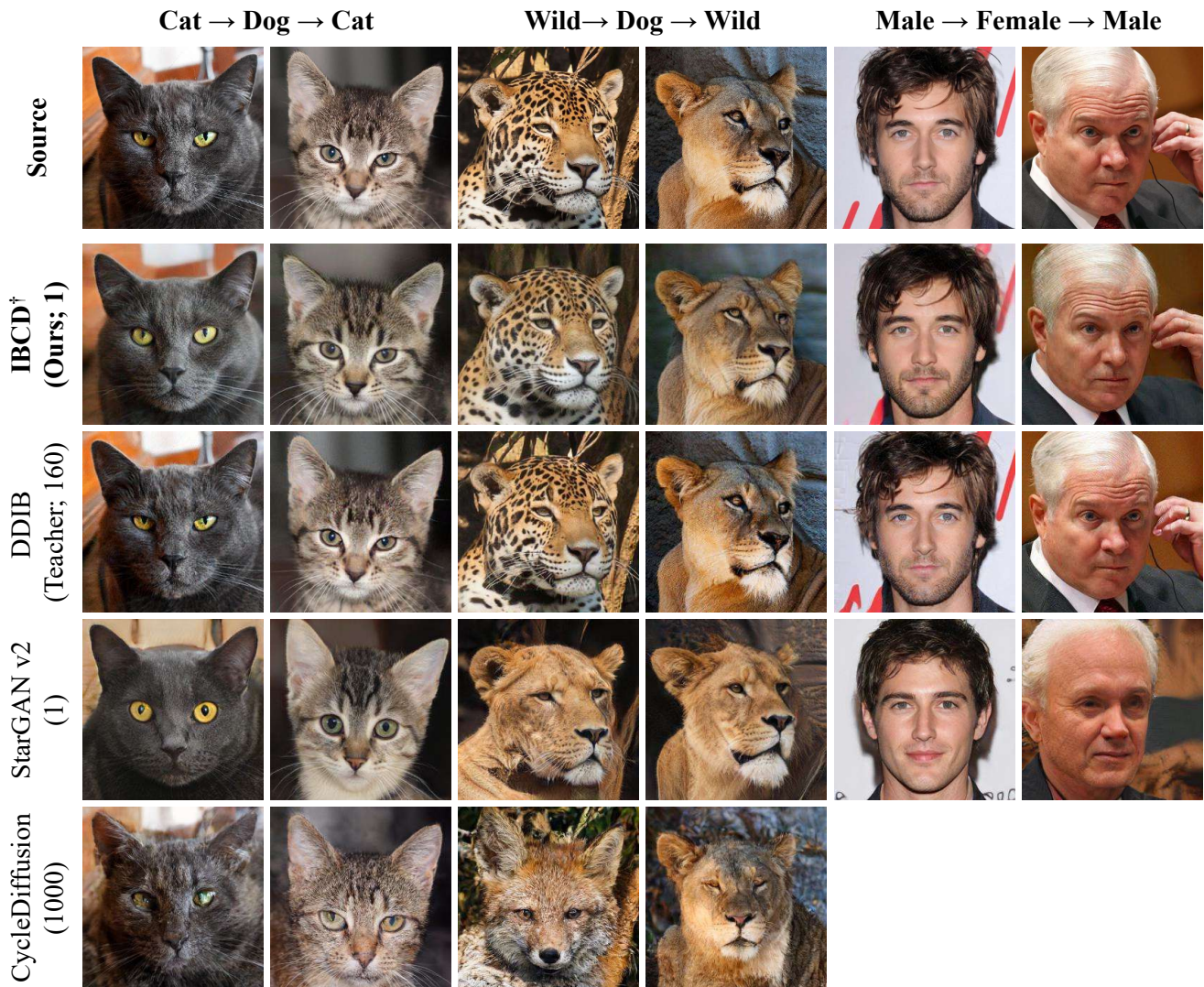


Figure 13. **Qualitative comparison of unpaired image-to-image translation tasks (cycle translation).** Compared to other baselines, our model achieves consistent cycle translations in a single step. The numbers in parentheses represent inference NFE.



Figure 14. Result of the bi-directional cycle translation with a single model for the Cat ↔ Dog task (IBCD[†]).



Figure 15. Result of the bi-directional cycle translation with a single model for the Wild↔Dog task (IBCD[†]).



Figure 16. Result of the bi-directional cycle translation with a single model for the Male↔Female task (IBCD[†]).